Experimental Results on Charge-Changing Collisions of Hydrogen and Helium Atoms and Ions at Kinetic Energies above 0.2 kev*

SAMUEL K. ALLISON

Enrico Fermi Institute for Nuclear Studies, University of Chicago, Chicago, Illinois

TABLE OF CONTENTS

I. INTRODUCTION

THE presence of a magnetically nondeviable constituent of the "canal rays" was observed by the experimental physicists of the last decade of the 19th century. This constituent was soon correctly interpreted as formed by ions which had been electrically charged when accelerated toward the cathode but had neutralized themselves while in motion by impacts with the surrounding gas molecules. As nearly as 1908 we find these ideas clearly stated by Wien (Wi 08, 11, 12),[1] and differential equations written down representing the changing charge composition of an ion beam in terms of mean free paths in the gas per electron

* This work was supported in part by the U. S. Atomic Energy Commission, Contract No. AT(11-1)238.

[1] References are listed at the end of this article on p. 1167.

capture and loss (cf. Rü 33). Quantitative information concerning these mean free paths proved very difficult to obtain, and it is doubtful whether any reliable data concerning the phenomenon were obtained before 1920.

This article is limited to the experimental results on charge-changing collisions of hydrogen and helium atoms and ions. Scattered data exist on these phenomena for other ions in motion, but are not included. Theoretical attempts to compute the charge-changing cross sections are not discussed, but a list of theoretical papers is given as a separate bibliography.[2]

The first precise experiments on charge-changing collisions resulted from the observation by Henderson (He 22), in 1922, that alpha particles emitted from a radioactive source and deviated in a magnetic field always show evidence of a singly as well as a doubly charged component. This discovery was followed up by Rutherford, who measured the equilibrium fractions of He^+ present in α-particle beams which had traversed thin foils; and also obtained some capture cross sections σ_{21} in air. (Ru 24). Other early papers were by Henderson (He 25), Briggs (Br 27), Kapitza (Ka 24), and Jacobsen (Ja 27). This work on α particles of energies ranging from 406 to 7680 kev is reported by Rutherford *et al.* (Ru 31a), and some of the numerical results are included here.

The first quantitative work on proton beams in the energy range of this review seems to have been by Bartels (Ba 30). Reviews of the status of the problem in 1933 appeared in *Handbuch der Physik* (Rü 33, Ge 33). Theoretical attempts to calculate electron capture probabilities using classical electrodynamics were made by Fowler (Fo 24) and by Thomas (Th 27). The earliest theories based on wave mechanics were published by Oppenheimer (Op 28) and by Brinkman and Kramers (Br 30).

Work on the problems of hydrogen and helium charge exchange in the pre-war period 1931–1941 has been extensively summarized by Massey and Burhop (Ma 52). During this period Wolf (Wo 36, 36a, 37, 37a) performed many experiments concerned with this phenomenon in the energy range 0.030 to 1.03 kev, and Rostagni (Ro 34, 35, 36, 38) worked approximately in the same energy interval. The work of these two investigators has not been separately reported here; above 0.2 kev the later work of Hasted and of Stedeford (Ha 55, St 55) covers the same region and, in general, makes a satisfactory junction with higher energy data. During this period the work of Meyer (Me 37, 40) is outstanding in that he pushed the kinetic energies up to 200 kev, but his results are often widely at variance with more recent data, indicating the presence of systematic errors.

Smith (Sm 34) made measurements of σ_{10} for H^+ ions traversing the target gases hydrogen and helium, and for He^+ ions in helium. His energy range was from 2 to 12 kev, and for the lower third of this range his results are not in significant disagreement with those tabulated here.

The period following World War II has been characterized by greatly increased experimental activity in this field, particularly in the kinetic energy range of interest here. In several ways, the experiments at kinetic energies below the kilovolt region are more difficult to interpret than are those at higher energies. In measurements in gases the relative prevalence of elastic collisions resulting in large angular deviations confuses measurements of beam attenuation, and the penetrating power of the ions in solids is so small that suitable foils are not readily obtained.

The study of the higher energy region was also facilitated by the fact that Cockcroft-Walton accelerators, originally constructed for researches in nuclear transformations or as neutron generators, had become somewhat outmoded for these purposes and could be used for charge-changing and stopping power researches. Thus we find a group at the University of Chicago making studies in the 50 to 450 kev region, and an Oak Ridge group working up to 200, and with a Van de Graaff generator, up to 1000 kev. In England, at University College, London, investigations in the energy range 0.1 to 40 kev have been carried out. In the period 1945–1955 the bulk of the experimental work on this problem has been done at these three locations. The experimental situation as of 1953 was reviewed by Allison and Warshaw (Al 53) and by Geller (Ge 55). During the last 4 years, contributions have been made from Russian groups at Leningrad and Kharkov.

II. MATHEMATICAL DESCRIPTION OF CHARGE CHANGING

A. Charge-Changing Probabilities in a Three-Component System

It has become customary to express the probability of a charge-changing collision by a cross section σ_{if} where i represents the initial charge of the moving ion in units having the magnitude of the electronic charge, and f is the charge after the event. The symbol presumes to represent the total cross section for charge changing, so that if every beam particle whose charge is changed is at once removed from a unidirectional beam, σ_{if} is the cross section for attenuation by change of charge. If one should take account of the angle of scattering of the beam particle in the charge-changing collision, $d\sigma_{if}/d\theta$ would be a function of angle. Some measurements (Ca 56, Fe 58, etc.) have been reported on the probability of scattering, accompanied by charge change $i \rightarrow f$, and into unit solid angle at angle θ, thus constituting direct measurements of $d\sigma_{if}/d\Omega$. In terms of this quantity

$$\sigma_{if} = 2\pi \int_0^\pi [d\sigma_{if}/d\Omega] \sin\theta d\theta, \qquad \text{(II-1)}$$

[2] Bibliography of theoretical papers will be found on p. 1168.

but σ_{if} has not as yet been measured by computational integration of differential cross sections measured at various angles.† Unless $|f-i|$ is large; and certainly for collisions involving the capture or loss of one electron with i small, the bulk of the contribution to σ_{if} is at negligibly small scattering angles since the only effective momentum interchange is with a loosely bound electron.

The experimental methods described in Sec. III are such that the integration of Eq. (II-1) is performed by the apparatus, method, and geometry of the measurement. For instance, many of the experimental researches reviewed here were attenuation measurements on ion beams moving in strong transverse electric or magnetic fields, so that those ions changing charge were removed by the field, and failed to enter a collecting aperture. This method, if properly applied, will measure a cross section at least as large as the cross section σ_{if}. The uncorrected result of the experiment may be too large if it has not been demonstrated that there is zero attenuation in the absence of the field, i.e., no appreciable large-angle scattering from any cause.

In another method of measurement one observes the excess of positive over negative target gas ion current produced in unit path length of the ion beam; in the case of single electron capture ($f=i-1$), σ_{if} is directly calculable from the result, since the capture of an electron leaves an uncompensated positive ion in the gas. In this method again, the integration over all angles is obviously incorporated.

The experimental difficulties, and complexity of the mathematical description of the beam composition, increase very rapidly with the number of components which must be considered. The number of components is simply the number of charge states that contribute significantly to the phenomena in question. If one begins an experiment with 1000 kev protons, and does not degrade their energy, it is clear that a two-component system comprising H^0 and H^+ is sufficient. Since only the hydrogen charge types H^-, H^0, H^+ are known, hydrogen is at most a three-component system. Although recently it has been found that He^- is a minute but observable constituent in helium beams, its interaction with the other charge states can be treated as a perturbation on the three-component He^0, He^+, He^{++} system.

As an extreme case, one might imagine the preparation of a pure He^- beam, its acceleration *in vacuo* to kinetic energies of several hundred kilovolts, and then its passage through a gas collision chamber. Over a very small pressure range, comparable amounts of all four charge states He^-, He^0, He^+, He^{++} might be found, but He^- would not be regenerated from its daughters, and subsequent to its very rapid decay the beam would continue as a three-component system.

The charge states of the three components can be designated as $i-1$, i, and $i+1$, with $i=0$ for the hydrogen system and 1 for the helium system. We will write out the equations for the helium system; they transform to the hydrogen system through the reduction of each finite numerical subscript by unity.

There are six charge-changing cross sections for the helium three-component system. Since an attenuation experiment measures the sum of the probabilities of the two possible charge-changing events for each ion type, it is convenient to introduce

$$\alpha \equiv \sigma_{01}+\sigma_{02}, \tag{II-2}$$

$$\beta \equiv \sigma_{10}+\sigma_{12}, \tag{II-3}$$

$$\gamma \equiv \sigma_{20}+\sigma_{21}. \tag{II-4}$$

We use π to represent the number of atoms of target gas per cm² which the beam has traversed. If, as in the usual experimental situation, the beam passes from high vacuum into, and exists into high vacuum from, a compartment of length l which contains an elementary gas having ξ atoms per molecule, at pressure P dynes/cm², then

$$\pi = Al\xi P/RT, \tag{II-5}$$

where A is Avogadro's number, R the gas constant (8.31×10^7 ergs/mole°C) and T the absolute temperature.

B. Differential Equations for a Three-Component System and Their Solution

The changing charge composition of a three-component ion beam may be expressed by the following equations:

$$dF_0/d\pi = -F_0(\alpha+\sigma_{20})+F_1(\sigma_{10}-\sigma_{20})+\sigma_{20}, \tag{II-6}$$

$$dF_1/d\pi = F_0(\sigma_{01}-\sigma_{21})-F_1(\beta+\sigma_{21})+\sigma_{21}, \tag{II-7}$$

$$F_2 = 1-(F_0+F_1), \tag{II-8}$$

where F_0, F_1, and F_2 are the fractions of the total moving beam to be found in the charge states 0, 1, and 2 at any point in the traversal of the target gas. We proceed by introducing four new constants which are linear combinations of the cross sections:

$$\begin{aligned} a &\equiv -(\beta+\sigma_{21}), \quad & f &\equiv (\sigma_{10}-\sigma_{20}), \\ b &\equiv (\sigma_{01}-\sigma_{21}), \quad & g &\equiv -(\alpha+\sigma_{20}). \end{aligned} \tag{II-9}$$

† *Note added in proof.*—Experimental results on large angle scattering of He^0, He^+, and He^{++} particles formed from an incident He^+ beam in the target gases He, Ne, and A have been reported by Fuls *et al.* (Fu 57). The measurements were made at 25, 50, and 100 kev kinetic energy; and the percentages of the various charge states in the scattered beams were determined, as well as the total differential cross section for all states at scattering angles up to 24° in the laboratory system.

In a paper to be published by Jones, Ziemba, Moss, and Everhart, special attention has been paid to measurements at small angles (below 4°), and some total cross sections have been determined by numerical integration. Total cross sections, σ_{10} and σ_{12} for He^+ in Ne and He target gases, and σ_{10} in A, thus obtained, show good agreement with those in Tables VI-6, VI-9, and VI-10, obtained by an entirely different experimental method.

The two independent differential equations become

$$dF_0/d\pi = gF_0 + fF_1 + \sigma_{20}, \quad \text{(II-10)}$$

$$dF_1/d\pi = bF_0 + aF_1 + \sigma_{21}. \quad \text{(II-11)}$$

The solution for F_i which is of physical interest may be expressed as follows:

$$F_i = F_i + [P(z,i)\exp(\pi q) + N(z,i)\exp(-\pi q)]\exp(-\tfrac{1}{2}\pi \textstyle\sum \sigma_{if}), \quad \text{(II-12)}$$

in which

$$q = +\tfrac{1}{2}[(g-a)^2 + 4bf]^{\frac{1}{2}} \quad \text{(II-13)}$$

and

$$\textstyle\sum \sigma_{if} = -(a+g). \quad \text{(II-14)}$$

$P(z,i)$ is a function of the cross sections applicable to a beam whose initial charge composition ($\pi=0$) is denoted by z, and of the ion charge (i) whose behavior in the beam is under consideration,

$N(z,i)$ is the analogous coefficient of the negative exponential.

C. Interpretation and Evaluation of the Constants of Integration

Initial conditions of special interest are those in which the ions of the beam, traveling in high vacuum before entering the collision compartment, are all of the same charge. Thus $P(0,1)$ represents the appropriate coefficient for the growth of He^+ in a beam which was originally 100% He^0.

In all cases of physical interest $\frac{1}{2}\sum \sigma_{if} > q$; otherwise some F_i would increase beyond all bounds. Thus, in the limit $\pi \to \infty$, the term in Eq. (II-12) involving exponentials becomes zero leaving

$$F_{i\infty} = \lim_{\pi\to\infty} F_i, \quad \text{(II-15)}$$

and $F_{i\infty}$ represents the fraction of ions of charge i in the beam after it has undergone a sufficient number of collisions so that no further change in charge composition can be detected. The equilibrium beam fractions $F_{i\infty}$ can be expressed in terms of the fundamental probabilities by equating Eqs. (II-6) and (II-7) to zero. The expressions are

$$F_{0\infty} = (f\sigma_{21} - a\sigma_{20})/D = (\beta\sigma_{20} + \sigma_{10}\sigma_{21})/D, \quad \text{(II-16)}$$

$$F_{1\infty} = (b\sigma_{20} - g\sigma_{21})/D = (\alpha\sigma_{21} + \sigma_{01}\sigma_{20})/D, \quad \text{(II-17)}$$

$$F_{2\infty} = [\sigma_{20}(a-b) + g(a+\sigma_{21}) - f(b+\sigma_{21})]/D, \quad \text{(II-18)}$$

in which

$$D = ag - bf = \sigma_{12}(\alpha+\sigma_{20}) + \sigma_{10}(\gamma+\sigma_{02}) + \alpha\sigma_{21} + \sigma_{01}\sigma_{20}. \quad \text{(II-19)}$$

The values of the constants $P(z,i)$ and $N(z,i)$ for a three-component system in which i and f can take on the values 0, 1, and 2 are given in Table II-1, for the cases in which an initially pure beam consisting entirely of ions with charge z in units of the magnitude of the electronic charge is allowed to enter a collision chamber. In this table the symbol

$$s \equiv \tfrac{1}{2}(g-a) \quad \text{(II-20)}$$

appears. The following relations between the P's, N's, and F's are apparent from the condition that at $\pi=0$ the beam consists of one charge component only

$$F_{i\infty} = -[P(z,i) + N(z,i)], \quad z \neq i, \quad \text{(II-21)}$$

$$1 - F_{i\infty} = [P(z,i) + N(z,i)], \quad z = i. \quad \text{(II-22)}$$

D. Transformation of the Equations to the Hydrogen Three-Component System

As they stand the equations thus far developed apply to a three-component system with charge states 0, 1, and 2, with the He^0, He^+, and He^{++} system as an example. The charge states appropriate to the hydrogen

TABLE II-1. Values of P and N of Eq. (II-12) for a three-component system with charge states 0, 1, 2.

Original state ($\pi=0$)	$P(z,i)$	$N(z,i)$
(A) To calculate changes in the fraction of He^+ present in a beam in which originally all the ions had the same charge.		
All He^0	$P(0,1) = \frac{1}{2q}[bF_{2\infty} + (b+s-q)F_{1\infty}]$	$N(0,1) = -\frac{1}{2q}[bF_{2\infty} + (b+s+q)F_{1\infty}]$
All He^+	$P(1,1) = -\frac{1}{2q}[(s-q)(1-F_{1\infty}) + bF_{0\infty}]$	$N(1,1) = \frac{1}{2q}[(s+q)(1-F_{1\infty}) + bF_{0\infty}]$
All He^{++}	$P(2,1) = \frac{1}{2q}[F_{1\infty}(s-q) - bF_{0\infty}]$	$N(2,1) = -\frac{1}{2q}[F_{1\infty}(s+q) - bF_{0\infty}]$
(B) To calculate changes in the fraction of He^0 present in a beam in which originally all the ions had the same charge.		
$z\lvert e\rvert$	$P(z,0) = P(z,1)(s+q)/b$, $z=0,1,2$	$N(z,0) = N(z,1)(s-q)/b$, $z=0,1,2$
(C) To calculate changes in the fraction of He^{++} present in a beam in which originally all the ions had the same charge.		
$z\lvert e\rvert$	$P(z,2) = -P(z,1)(b+s+q)/b$, $z=0,1,2$	$N(z,2) = -N(z,1)(b+s-q)/b$, $z=0,1,2$

system are -1, 0, and 1, and the equations can be made to apply to hydrogen beams by subtracting one from each finite index. As an example, from Eq. (II-16) we obtain, for the equilibrium fraction of negative hydrogen

$$F_{\bar{1}\infty}=(\beta\sigma_{1\bar{1}}+\sigma_{0\bar{1}}\sigma_{10})/D, \quad \text{(II-23)}$$

where

$$\beta=\sigma_{0\bar{1}}+\sigma_{01} \quad \text{(II-24)}$$

and

$$D=\sigma_{01}(\alpha+\sigma_{1\bar{1}})+\sigma_{0\bar{1}}(\gamma+\sigma_{\bar{1}1})+\alpha\sigma_{10}+\sigma_{\bar{1}0}\sigma_{1\bar{1}} \quad \text{(II-25)}$$

with

$$\alpha=\sigma_{\bar{1}0}+\sigma_{\bar{1}1} \quad \text{and} \quad \gamma=\sigma_{1\bar{1}}+\sigma_{10}. \quad \text{(II-26, 27)}$$

Furthermore, the values for P and N useful in calculating the growth of a H^- component from an initially pure H^+ beam may be obtained by transformation from Table II-1. They are (see also Table VI-16)

$$P(1,1)=\frac{s+q}{2qb}[F_{0\infty}(s-q)-bF_{\bar{1}\infty}], \quad \text{(II-28)}$$

$$N(1,\bar{1})=-\frac{s-q}{2qb}[F_{0\infty}(s+q)-bF_{\bar{1}\infty}]. \quad \text{(II-29)}$$

q and s are defined in Eqs. (II-13) and (II-20), but with β as in Eq. (II-24), and

$$\begin{aligned} a&\equiv-(\beta+\sigma_{10}), \quad f\equiv(\sigma_{0\bar{1}}-\sigma_{1\bar{1}}),\\ b&\equiv(\sigma_{\bar{1}0}-\sigma_{10}), \quad g\equiv-(\alpha+\sigma_{1\bar{1}}). \end{aligned} \quad \text{(II-30)}$$

E. Equations for a Two-Component System

There are wide areas of considerable interest in which equations for a two-component system are sufficient to describe the charge-changing behavior of hydrogen and helium beams. The behavior of a He^+ or He^0 beam, below 80 kev in kinetic energy, on entering a collision chamber is describable as that of a two-component (He^0, He^+) system with minute perturbations due to He^{++} ($\sim 0.2\%$) and He^- ($<0.1\%$), and above 50 kev H^- plays no significant role in the charge changing of beams originally either H^0 or H^+.

For a two-component system, with $i=0$, 1,

$$dF_0/d\pi=[1-(dF_1/d\pi)]=-F_0\sigma_{01}+F_1\sigma_{10}, \quad \text{(II-31)}$$

and this may be shown to be the consequence of setting $F_2=0$ in Eqs. (II-6) to (II-8). The solutions are

$$F_i=F_{i\infty}+P(z,i)\exp[-\pi(\sigma_{01}+\sigma_{10})], \quad \text{(II-32)}$$

with

$$F_{0\infty}=\sigma_{10}/(\sigma_{01}+\sigma_{10}); \quad F_{1\infty}=\sigma_{01}/(\sigma_{01}+\sigma_{10}). \quad \text{(II-33, 34)}$$

As before, the index z describes the initial condition ($\pi=0$) of the beam before undergoing charge-changing collisions, and the two important cases in which the initial beam is all neutral ($z=0$) or all singly charged ($z=1$) lead to the set of values in Table II-2.

TABLE II-2. Values of $P(z,i)$ in Eq. (II-32) for a two-component system with charge states $i=0$, 1.

Initial beam	$P(z,i)$	
All neutral	$P(0,0)=F_{1\infty}$	$P(0,1)=-F_{1\infty}$
All charged	$P(1,0)=-F_{0\infty}$	$P(1,1)=F_{0\infty}$

III. DEDUCTIONS FROM THE CHARGE-CHANGING EQUATIONS

A. Significance of a Maximum in the Growth of a Charge Component

Consider a prepared ion beam *in vacuo* in which all the ions have the same charge z. The beam is allowed to pass through a collision chamber and the fraction F_i of the ions emerging with charge i is examined as a function of pressure in the collision chamber. For a two-component system, F_i must be a monotonic function of π, but for a three-component system F_i may pass through a maximum at $\pi=\pi_m$. For instance, Windham *et al.* (Wi 58, see also Da 57) have observed a maximum in the production of He^- from a 17.5 kev He^+ beam emerging from a H_2 gas collision chamber.

By taking the derivative $dF_i/d\pi$ from Eq. (II-12), we find that if the F_i *vs* π curve has zero slope at finite π_m, π_m must satisfy the equation

$$\pi_m=\frac{1}{2q}\log_e\left\{\frac{[-N(z,i)/P(z,i)][\frac{1}{2}\sum\sigma_{if}+q]}{\frac{1}{2}\sum\sigma_{if}-q}\right\}. \quad \text{(III-1)}$$

We have seen (Sec. II-C) that $(\frac{1}{2}\sum\sigma_{if}-q)>0$, and that both $\frac{1}{2}\sum\sigma_{if}$ and q are positive. Thus, the necessary condition for a real extremum at some finite π_m is

$$N(z,i)/P(z,i)<0. \quad \text{(III-2)}$$

For example, if H^- is being produced from a 15-kev H^+ beam, by charge-changing collisions in a hydrogen gas collision chamber, the cross sections of the three-component system (Table V-8a) lead to the tabulated values (Tables V-17, V-18)

$$\begin{aligned} P(1,\bar{1})&=0.055, & q&=3.80\times10^{-17}\ \text{cm}^2,\\ N(1,\bar{1})&=-0.076, & \tfrac{1}{2}\textstyle\sum\sigma_{if}&=45.4\times10^{-17}\ \text{cm}^2, \end{aligned}$$

and substitution in Eq. (III-1) shows that a maximum output of H^- will be obtained at $\pi_m=6.4\times10^{15}$ atoms/cm^2, corresponding to a hydrogen gas pressure of about 10 μ in a collision cell 10 cm long at 20°C. The maximum is rather flat, however (see Fig. V-4), and not of great experimental importance.

B. Charge-Changing Cycles in a Two-Component System

Consider an ion of charge i in a two-component ion beam in which the two possible charge states differ by one electronic charge. Eventually the ion will undergo a charge-changing collision to the other component, of charge $i\pm1$, and subsequently, in a second such

collision, it will return to charge i, thus completing a charge-changing cycle. The result of this is to produce in the target gas an electron and a positive ion, the points of origin of the pair being on the average separated by the sum of the mean free paths for the two types of charge-changing events.

To avoid cumbersome and unnecessary generality, consider that the two components have charges 0 and 1. Then the number of electron-positive ion pairs formed in the collision chamber by the charge changing mechanism may be conveniently computed through the use of a cross section for cycle completion,

$$\sigma_c=\sigma_{01}\sigma_{10}/(\sigma_{01}+\sigma_{10}), \qquad \text{(III-3)}$$

which expresses the additivity of the corresponding mean free paths. Thus the average number of events, in which a neutral is produced, per proton traversing a collision chamber in which there are π atoms of gas per cm^2 in its path, is simply $\pi\sigma_c$.

C. Electron Capture in the Slowing Down of Protons: Application to Pionium and Muonium Formation

In the portion of its range in a gas in which the kinetic energy of a proton degrades from E_0 to E, the number of collisions in which neutral hydrogen atoms are formed is

$$N_c=L\xi\int_{E_0}^{E}\sigma_c(E)\frac{dE}{\epsilon(E)}, \qquad \text{(III-4)}$$

where $\epsilon(E)=dE/dx$ is the stopping power of the gas in kilovolts/cm under standard conditions and E and E_0 are to be expressed in kev. L is the number of molecules per cm^3 in a gas at standard conditions, and ξ is the number of atoms per molecule in the target gas in cases such as tabulated in this review where the cross sections are per *atom* of gas traversed. If the interval of integration E_0-E is widened, N_c approaches a finite asymptote, and one can speak of the total number of charge-changing cycles in the slowing down of a fast proton as a function only of the nature of the material traversed. Thus a proton of more than 300 kev initial kinetic energy makes about 680 charge-changing cycles in slowing down to 9 kev in hydrogen gas.

To the accuracy of the present considerations, deuterium, hydrogen, pionium, and muonium have the same ionization potential and may be considered hydrogen isotopes. The number of neutralizations in slowing down a hydrogen isotope is m/m_p times the number for hydrogen, where m is the isotopic and m_p the proton mass. Thus a fast positive pion catches and loses an electron 96 times in slowing down to 1.3 kev kinetic energy in hydrogen gas.

D. Time Spent as a Neutral Atom during the Slowing Down Process

The time spent in the neutral state in the slowing down of a singly charged ionic beam from E_0 to E in a target gas at p, T is

$$t_c=\frac{p_0T}{pT_0}\int_{E_0}^{E}\frac{\sigma_c}{\sigma_{01}}\frac{dE}{\epsilon(E)V(E)}, \qquad \text{(III-5)}$$

provided two charged components 0 and 1 are adequate to describe the beam. p_0 and T_0 refer to 76 cm and 273°K, respectively, and $V(E)$ is the speed of the beam particles in cm/sec. For a given target gas this time depends on p and T, but approaches an asymptote which depends on the lower energy limit E, and is independent of E_0. For the slowing down of a fast ($E\gtrsim 300$ kev) proton in hydrogen gas at 1 atmos and 20°C the time spent as a neutral is 1.21×10^{-9} sec if the lower energy limit is 9 kev. Thus the corresponding time for pionium to exist is 1.75×10^{-10} sec in the slowing down of a fast positive pion to a lower limit of 1.3 kev kinetic energy.

IV. EXPERIMENTAL METHODS

A. Calibration of Detectors for $F_{i\infty}$ Determinations

The fractions $F_{i\infty}$, defined in connection with Eq. (II-15) may be directly measured, or computed from a set of measured σ_{if} values. In essence, the measurement consists in the charge analysis of a beam which has been brought to charge equilibrium by the traversal of sufficient material. If the beam has been equilibrated by passage through a solid foil, or by scattering from a solid, the charge analysis may be readily carried out in high vacuum.‡

If the beam has been equilibrated by traversing a gas, analysis of its charge composition may be made in the gas itself, or in a compartment where high vacuum is maintained through differential pumping. In the energy range up to 450-kev hydrogen and helium beams are charge equilibrated in passage through 10^{-5} to 10^{-4} mg/cm^2 of gas; therefore, it is impractical to separate pressure compartments by foils without imposing on the beam the charge equilibrium characteristic of the foil. An experimental arrangement is outlined in Fig. IV-1.

Almost all experiments on charge changing involve the properties of a narrow ($\sim$0.1 cm^2 cross section), approximately unidirectional ion beam which passes through several apertures, and finally, through a small opening into a detector.

‡ In this type of experimentation, high vacuum means a pressure at which the mean free path between charge-changing collisions is perhaps 100 times as long as the beam path length in the measuring chamber. This means that 5×10^{-6} mm is sufficiently low for even the most probable events.

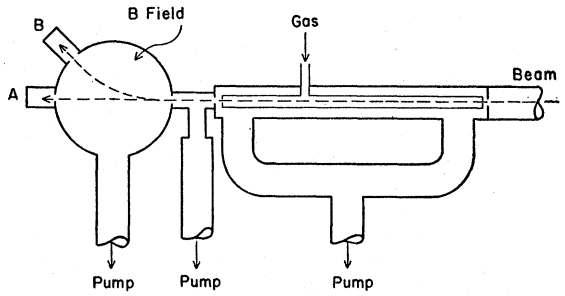

FIG. IV-1. An experimental arrangement in which the fractions $F_{i\infty}$ are measured in high vacuum. The charged beam enters from the right, and is equilibrated in the inner gas cell. The neutral component is measured in a detector at A; the charged components are directed to B by suitable changes in the magnetic field.

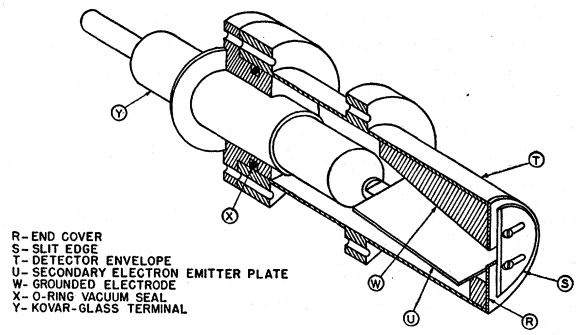

FIG. IV-2. An ion beam detector used by Montague (Mo 51) in a region where there is a stray magnetic field. The magnetic lines of force are approximately normal to the secondary emitter plate U. U and W are separated by about 5 mm.

In most equilibrium fraction measurements, the various charge states are spread out into a charge spectrum, by an electric or magnetic field, and by various devices the flux of ions in each separated beam is measured. An obvious source of error arises if there should be a mechanism, operating in the equilibrating region, which preferentially removes one charge state from the unidirectional beam. For instance, if the component He^{++} had an elastic scattering cross section larger than that of He^0 for scattering into angles which would remove it from the detector aperture, too low a value for $F_{2\infty}$ would be observed. Stier and Barnett (St 56) and Fogel *et al.* (Fo 57) have carried out tests to determine whether such an effect was vitiating their experiments. Both tests consisted essentially in determining that the emergent beam was of uniform composition at right angles to the direction of propagation. Stier and Barnett passed a narrow slit across the beam and determined attenuation coefficients in the thin slices selected from the center and peripheral portions of the beams. In a beam of H^0, of kinetic energy 4 kev, passing through nitrogen, the peripheral portions seemed to have a slightly higher H^+ component than the central, as if collisions accompanied by significant angular deviation and by the electron loss from H^0 were more prominent than such collisions in which $H^+ \rightarrow H^0$. No such effect was observed above 10 kev in kinetic energy and no appreciable correction to the average composition across the beam was needed.

It is also necessary to demonstrate that the detecting devices truly measure the flux of ions in the beam, and if the detector response is different for two beams of the same kinetic energy, having the same flux of ions but of different charge, the nature of the charge dependence must be known. If one of the beams to be measured is electrically neutral, it is clear that a Faraday cup detector cannot be used.

A type of detector whose response (at beam energies in the kilovolt region) is certainly unaffected by the ionic charge is a thermocouple or thermister which measures the rate of generation of heat in a target of low heat capacity bombarded by the beam. To a higher degree of accuracy than is now attained in charge-changing experiments the beams containing the various charge components have the same kinetic energy per ion. Detectors of this type have been used by Rudnick (Ru 31), Snitzer (Sn 53), Stier *et al.* (St 54), and others. A disadvantage of such calorimetric detectors is that the attainment of radiative equilibrium is delayed due to the heat capacity of the detector itself. This is particularly serious if the flux of the beam from the ion accelerator is not constant. If two detectors are used, one for the neutral and one for the charged beams, the temperatures of the housings around the detectors must be controllable and known.

Probably the most widely used detector is the secondary electron emitter, which will give a response to a neutral beam. Such a detector, as used by Montague (Mo 51) is shown in Fig. IV-2. The question of the charge dependence of a secondary electron detector has been investigated by Barnett and Reynolds (Ba 58). The secondary electron emitter was a brass surface, and the true ratio of the beam fluxes incident upon it was determined calorimetrically. The H^0 beam ejected more electrons per incident particle than did a H^+ beam of the same kinetic energy per particle. The ratio of the response varied from 1.37 at 200 kev to 1.62 at 1000 kev in a linear increase as a function of energy. Due to the complicated nature of secondary electron emission, and its dependence on the nature and past history of the surface, it would be dangerous to generalize this result, but at least equal response, irrespective of charge, cannot be taken for granted.

However, the entire question of the charge dependence of detector response can be obviated by equilibrating the beam charge in a thin foil just before the beam impinges on the secondary electron emitting surface (cf. Al 53, p. 809). For instance, an ion beam component of the separated charge spectrum may be made to pass through a thin gold foil before impinging on a beryllium-copper electron emitting surface (Al 58) which is negatively biased so that electrons from the foil cannot reach it. Then, irrespective of the charge

per ion of the beam component, the same charge mixture is incident on the secondary emitter, since this is a function only of the material of the foil and the kinetic energy in the beam. If the arrival of each individual particle at the detector is counted, as in the scintillation experiments of Rutherford (Ru 24), the difficulties of detector calibration are, of course, obviated. However, it is not always easy to reduce the intensity of ion beams from an accelerator to the point where counting without pile-up is feasible without introducing other undesireable features into the experiment.

In measuring the two values of $F_{i\infty}$ appropriate to an equilibrated two-component system, it is, in principle, only necessary to use one stationary detector. If one of the components has $i=0$, the fraction $F_{0\infty}$ can be determined by allowing the entire equilibrated beam to strike the detector; followed by a reading in which the charged component has been removed by the application of a field. If neither value of i is zero, the situation is more flexible; each component may be separately directed to the detector and measured.

In order to direct the various beams to the detector, various values of the directing field (electric or magnetic) must be used, and it must be demonstrated that changing the field did not affect the detector response. Actually, the difficulty need only arise if a magnetic deflection is used, since it is notoriously difficult to eliminate stray magnetic effects.

The Montague detector of Fig. IV-2, is so designed that the plane, parallel, electron emitting and collecting surfaces, have a lateral extent large compared to the small area hit by the beam and are oriented almost at right angles to the lines of force of the magnetic field which strays beyond the edge of the magnet. Thus, the lines of force of the electric collecting and biasing field are almost parallel to those of the stray magnetic field, if it be present. The secondary electrons, which move only a few millimeters from emitting to collecting surface, experience little force from the magnetic field.

In a three-component system, either the detector must be movable from beam to beam or at least two detectors must be used. In the case of a secondary electron detector, it is highly desirable that this motion be carried out in the high vacuum to avoid changing the emission characteristics through exposure to gas. Such a movable detector, at the end of a flexible bellows, was used by Stier and Barnett (St 56) in investigations of the hydrogen three-component system. Allison (Al 58) used two Montague detectors for the helium system, and devised the following tests of their relative sensitivity, the principal factors in any difference being undoubtedly different secondary electron yields. Both detectors had equilibrator foils as described previously. In the first test a beam consisting of approximately 90% He^{++}, 8.5% He^{+}, and 1.5% He^{0} was measured in detector A, in the absence of a magnetic field (cf. Fig. IV-1). The detector current I_A in this case is aN where a is the sensitivity factor of the detector and N the total particle flux. Subsequently first the He^{++} component and then the He^{+} were magnetically directed to the B detector, giving responses $I_B{}^{++}$ and $I_B{}^{+}$ equal to bF_2N and bF_1N, respectively. Since the beam is practically all He^{++}, we have, approximately,

$$(b/a)=(I_B{}^{++}+I_B{}^{+})/I_A. \qquad \text{(IV-1)}$$

A better value of (b/a) may be obtained by using this first estimate to correct for the small He^{0} beam. Such a calibration does not, however, demonstrate that the detector response is independent of stray magnetic fields in the detectors.

During the second test the detectors, which could be slipped out of cylindrical slots in the wall of the vacuum chamber between the magnet pole-pieces, were interchanged. Before the interchange, we had, from test 1,

$$(I_B{}^{++})/(I_A)=(b/a)F_2. \qquad \text{(IV-2)}$$

In the subsequent discussion of the situation following the interchange of detectors, we use the subscripts A and B as pertaining to the detectors of the first test themselves, and not as identifying the locations in Fig. IV-1 in which they operated after the interchange. Thus, after the change, the component He^{++} could be directed toward detector A, and subsequently, with the magnetic field off, the entire beam was read in B, giving

$$(I_A{}^{++})/(I_B)=(a/b)F_2 \qquad \text{(IV-3)}$$

from which one can calculate the relative sensitivity

$$(b/a)=[(I_B{}^{++}/I_A)\times(I_B/I_A{}^{++})]^{\frac{1}{2}} \qquad \text{(IV-4)}$$

it only being necessary to assume that if there is an effect of the magnetic field on the detectors, it is the same for both.

If the relative detector sensitivities resulting from the two tests agree, it may also be concluded that there is no significant magnetic effect on them, and that their secondary electron emission is not affected by brief exposure to air.

The above is an illustration of a calibration in which only the ratios of the secondary electron emissions from the two detectors need be measured; a straightforward method such as the calibration of each detector separately against an absolute detector, such as a thermocouple, would be logically less intricate but probably experimentally more laborious. It has usually been tacitly assumed that the ion current brought to the emitting surface by the beam is negligible compared to the secondary electron current drawn from the surface. If the errors in measurement now commonly admitted ($\sim$5%) are to be significantly reduced, and secondary electron detectors are used, the number of secondaries per primary ion will have to be more carefully investigated.

Experiments on charge-changing events in gases are commonly performed at pressures in the range 5×10^{-6}

to 5×10^{-2} mm of mercury, and the definitive pressure measurements made with a McLeod gauge, which must be separated from the equipment by a cold trap since at room temperature the vapor pressure of mercury lies within the range of measurement.

In measurements in gases, differential pumping to maintain a pressure drop from pressures in the collision chamber (10^{-4} to 10^{-2}) to "high" vacuum ($\sim5\times10^{-6}$) is used. The differential pumping compartments provide for beam entrance and exit through cylindrical apertures of a few mm diameter, and perhaps several diameters long. Pressure drops of 10- to 100-fold may be maintained across such apertures.

The beam and detector currents lie between 10^{-11} to 10^{-7} amp, a range which offers little experimental difficulty with modern equipment.

A few measurements of charge equilibria produced in solids have been carried out. In the case of hydrogen beams, the equilibria were produced by the passage through a thin foil, and in some of the older measurements on α particles from radioactive substances mica foils were used. At somewhat lower energies, helium beams have been charge equilibrated by scattering from a solid.

B. Measurements of Cross Sections σ_{if}

(1) *Measurement of Capture and Loss Cross Sections in a Two-Component System*

All measurements giving information on individual cross sections σ_{if} involve investigation of phenomena occurring in some transient stage of the process of charge equilibration of an ion beam. The fractions $F_{i\infty}$ are dimensionless, and only determine cross-section ratios. At the present time nothing is known of cross sections in solids. The following method is applicable to a two-component system in a gas and has been used in measurements of σ_{01} and σ_{10} in hydrogen beams. Using a prepared, pure beam (for convenience, this is usually a proton beam), one measures a value of F_1 and its associated π in a collision chamber in which the pressure is too low to equilibrate the beam, or at a point in traversing the gas too near the point of entrance into the gas for charge equilibrium to have been reached. Subsequently an equilibrium measurement is made to give $F_{1\infty}$. From Eqs. (II-32), (II-33), (II-34), and Table II-2, it may be shown that

$$\sigma_{01}=\frac{F_{1\infty}}{\pi}\log_e\left\{\frac{1-F_{1\infty}}{F_1-F_{1\infty}}\right\} \qquad \text{(IV-5)}$$

$$\sigma_{10}=\frac{1-F_{1\infty}}{\pi}\log_e\left\{\frac{1-F_{1\infty}}{F_1-F_{1\infty}}\right\}. \qquad \text{(IV-6)}$$

These equations were first devised by W. Wien (Wi 12).

This method probably requires less instrumentation than others subsequently described. The prepared proton beam may enter a simple collision chamber,

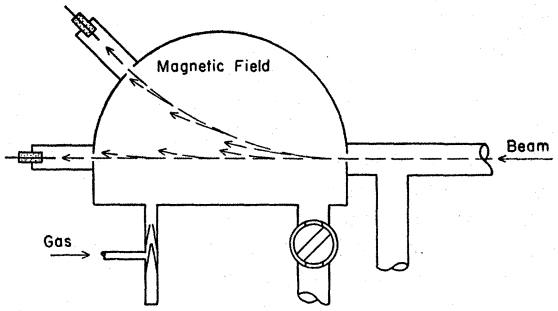

FIG. IV-3. Measurement of the attenuation due to charge exchange with ionic and atomic beams moving in a gas and in the presence of a transverse magnetic field.

at the far end of which is a Faraday cell detector. With high vacuum in the collision chamber the Faraday cell current gives the total beam flux. At some intermediate pressure π the cell current, divided by that at $\pi=0$, gives F_i since the atomic component contributes no current and finally, when the Faraday cell current is no longer a function of π, $F_{i\infty}$ is determined. With certain obvious changes, the set of readings can also be used if both beam components are charged. The method has been applied by Bartels (Ba 30), Meyer (Me 37), and others.

(2) *Measurements by Attenuation in a Transverse Field*

A method which does not involve the measurement of the quantities $F_{i\infty}$ is to place the collision chamber in a magnetic or electric field whose lines of force are perpendicular to the direction of motion of the beam in the absence of the field as in Fig. IV-3. The beam incident on the gas chamber, which is now being used for cross-section measurement, may be pure or mixed in its charge states; they are of course separated out into distinct beams in the field. With $\pi=0$ in the chamber, values of the deflecting field and locations of the detectors are found such that the various beams enter their detectors through apertures which are larger, but of diameter comparable to that of the beam itself. When gas is admitted to the chamber, each beam particle whose charge is changed is lost to the beam because it can no longer continue in its old orbit, and a beam attenuation due to charge changing is observed. Mathematically this is equivalent to imposing on the generalized form of Eq. (II-31) the condition that one F_i is zero for all values of π; the expression then degenerates into one which has as a solution

$$\sigma_{if}=-(1/\pi)\log R_i, \qquad \text{(IV-7)}$$

in which $R_i(\pi)$ is to be interpreted as the ratio of the detector response with gas in the chamber to the response which it had at high vacuum.

In this type of measurement, the effect of stray magnetic or electric fields on the detector need not be considered, since the only change in the experimental conditions during a measurement cycle is in the gas

pressure. It must be demonstrated however that the admission of sufficient gas for a measurable beam attenuation does not affect the response of the detector (Mo 51, Ri 51). Furthermore it must be shown that the beam, with gas in the chamber, is not appreciably attenuated by elastic scattering, or by any type of angular deviation not caused by the effect of the field on the ion whose charge is changed. This is usually demonstrated by turning off the field and allowing the beam to proceed in a straight line through the collision chamber to a detector with the same entrance aperture, and so placed that the length of path in the chamber for the straight (no-field) beam is the same as that for the component beam held in a curved orbit. Gas is then admitted as if an attenuation experiment were in progress in a field-directed beam. Fortunately, the charge-changing cross sections are usually so large compared to those resulting in angular deviations (without charge change) which would remove the particle from the beam, that it can be demonstrated in this way that no attenuation would be observed in the absence of the guide field. Another source of error arises if the differential pumping is not adequate, that is, if admission of the gas for the attenuation measurement should significantly increase the pressure in the compartments through which the beam passes prior to its entry into the measuring chamber. If by such an effect the charge composition of the entering beam is changed by the admission of gas to the measuring chamber, the cross section will be in error (Al 58).

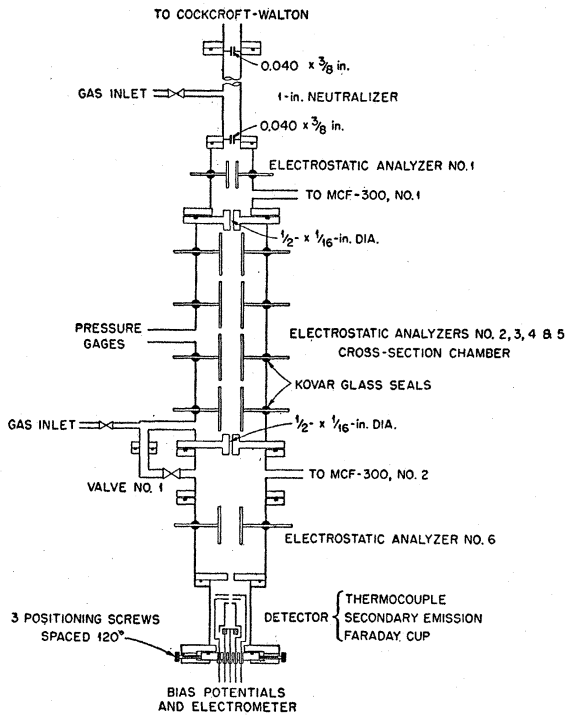

FIG. IV-4. Apparatus of Stier and Barnett for charge-changing measurements.

The background reading of the detector must be investigated with and without gas in the chamber used for the attenuation measurement. In the case of a charged beam, the profile of the beam may be easily observed by varying the guide field slightly so that the beam moves across, and slightly to one side of, the detector aperture. In the case of measurements on a neutral beam this cannot be done; the profile is examined by a movable slit in front of the detector (St 56, Al 58) or by a movable detector. If other beams than the one being measured are traversing the attenuation chamber, the ion spray from charge-changing collisions of these beams may introduce a large error by raising the background effect with "gas in" (Al 56).

Figure IV-4 shows an experimental arrangement in which the transverse "guide" field is electric, but, since the experiment is designed to study electron loss from neutrals, the field does not actually guide, it only removes charged ions as fast as they are formed. The segmentation of the electric field is partially to enable a better measurement of the l of Eq. (II-5), since through a series of measurements, using fractional parts of the total condenser length, a set of simultaneous equations can be found from which the additional Δl, the edge effect at the condenser entrance and exit, may be eliminated (Ka 57, St 56).

In Fig. IV-4 some of the charged particles from the Cockcroft-Walton accelerator (top) are allowed to neutralize themselves in the neutralizer cell. Any remaining charged particles are removed in "electrostatic analyzer No. 1," so that a pure neutral beam enters the "cross-section chamber" through the $\frac{1}{2}\times\frac{1}{16}$ in. cylindrical differential pumping aperture. The detector was sufficiently far away (1 m) so that a slight electric field was sufficient to prevent positives formed in the cross-section chamber from being measured. Obviously, the potentials required on the electric deflector plates must be low enough so that no glow discharge forms in the gas.

(3) Measurements of Capture Cross Section by Ion Collection

It is obvious that electron capture by a fast moving positive ion traversing a gas must leave behind a positive ion with a low kinetic energy except in the rare case where the impact parameter between the colliding atoms is small enough to transmit appreciable velocity to the secondary. Since the process of ionization of the target gas, if present, produces ion pairs in equal numbers, an excess of positive over negative ion current from the target gas can be interpreted in terms of electron capture (cf. Ma 52, pp. 499–500). The method has been used by Rostagni (Ro 38), Keene (Ke 49) and Kasner and Donahue (Ka 57).

For a simple interpretation it is essential that the only charge-changing process occurring in the volume of the target gas from which ions are swept out is

electron capture and that the number of electrons captured in a single collision is known. Therefore, if the method is used to measure σ_{10} for protons, it must be certain that a pure proton beam, unaccompanied by any neutral atoms, is incident in the collision chamber, and that the pressure is so low that no appreciable number of neutrals can have formed in the chamber and are passing through the measuring volume. The collecting plate or plates on which the slow ions are measured must be guarded against secondary electron emission caused by ultraviolet light in the gas, and from the collection of secondary electrons from slits and other surfaces exposed to the beam.

C. Measurement of Cross Sections in a Three-Component System

In a three-component system, such as helium in the kinetic energy region of a few hundred kilovolts, six charge-changing events are possible; as exemplified in this case by the cross-sections σ_{01}, σ_{02}, σ_{10}, σ_{12}, σ_{20}, σ_{21}. Two of these involve capture or loss of 2 electrons in one collision. In this more complicated system, some of the methods for cross-section measurement described in Sec. IV-B for a two-component system become inapplicable; for the others, the interpretation of the result must be reinvestigated. The first method under Sec. IV-B involving only beam composition determinations in a transient stage and at complete equilibration, has not been used in three components. Equations (II-12) are actually very elaborate combinations of the six cross sections; much more complex than the simple two-component expressions in (II-32). Many measurements would be necessary to evaluate all the integration constants.

The second method described in Sec. IV-B, in which the collision chamber is in a strong transverse field, and the attenuation of the ion beams is measured as change of charge results in departure from the orbit, does not measure any single cross section in a three-component system. What is measured is the total attenuation cross section for all possible charge-changing processes within the system, i.e., attenuation experiments on H^-, H^0, H^+ beams would give

$$(\sigma_{\bar{1}0}+\sigma_{\bar{1}1}),\quad (\sigma_{0\bar{1}}+\sigma_{01}),\quad \text{or}\quad (\sigma_{\bar{1}0}+\sigma_{10}),\qquad \text{(IV-8)}$$

respectively. Auxiliary experiments must be performed to separate these sums into individual cross sections.

The method of collection of ions formed in the target gas is also unsuitable for the determination of individual cross sections in a three-component system. Thus, if doubly charged ions such as He^{++} were being measured, and the cross-section σ_{20} were appreciable (which possibility cannot be *a priori* discarded), each such double capture event would be counted twice, and the cross section thus measured would be $(\sigma_{21}+2\sigma_{20})$ (cf. St 56, p. 907).

The auxiliary experiment necessary to obtain individual cross sections in a three-component system, once sums such as in (IV-8) are known, is essentially to prepare a beam consisting of only one charge state pass it through a collision chamber, and study the fractions F_i of the new charge states as they appear in the emergent beam at the lowest possible pressures. These pressures must produce values of π [Eq. (II-5)] so low that the probability that a beam particle can have more than one atomic collision during its traversal of the collision chamber is negligibly small. Under this circumstance only those charge states which can be produced in one collision will appear in the emergent beam, and the initial rate of their growth will be linear with π. Thus the initial growth of H^- and H^+ from a pure H^0 beam, or of He^0 and He^{++} from He^+, would certainly be linear, and in the helium case, for instance, the observed ratio F_0/F_2 would be equal to σ_{10}/σ_{12} which, together with an attenuation experiment to give $(\sigma_{10}+\sigma_{12})$, would suffice to determine the two cross sections themselves.

This procedure, namely, the investigation of the initial growth of new charge components from a pure original, has been used by Fogel and Mitin (Fo 56), to obtain the cross-section $\sigma_{1\bar{1}}$ in the H^-, H^0, H^+ system, and later (Fo 57) to obtain $\sigma_{\bar{1}1}$. If the growth of H^- from an originally pure H^+ beam can only proceed through the intermediate stage H^0, the initial stages will be proportional to π^2; if the process $\sigma_{1\bar{1}}$ is also possible, the growth of H^- will have both a linear and a parabolic term in π. For instance, Fogel and Mitin (Fo 56) give for the growth of H^- from H^+ the following formula, neglecting terms higher than π^2 in order:

$$F_{\bar{1}}=\pi\sigma_{1\bar{1}}+\tfrac{1}{2}\pi^2(\sigma_{10}\sigma_{0\bar{1}}+\sigma_{1\bar{1}}\sigma_{10}+\sigma_{1\bar{1}}{}^2-\sigma_{1\bar{1}}\sigma_{\bar{1}0}-\sigma_{1\bar{1}}\sigma_{\bar{1}1})+\cdots. \qquad \text{(IV-9)}$$

By finding the values of m and n in $(m\pi+n\pi^2)$ such that the experimentally observed growth curve of H^- from a pure H^+ beam is most closely represented, a value of $\sigma_{1\bar{1}}$ can be found from the linear term.

In the process of finding the best analytical expression for an experimental curve, great care must be taken to treat properly the errors in the experimental results the plot of which makes up the observed curve; and over a limited range it is difficult to separate the linear and parabolic components of a curve.

In an attempt to measure σ_{20} for He^{++} ions, Allison (Al 58) first measured $(\sigma_{20}+\sigma_{2\bar{1}})$ in a simple attenuation measurement on a He^{++} beam, as in the discussion preceding Eq. (IV-8). Then the He^{++} beam was passed through a collision chamber and as the components He^0 and He^+ grew from it, their ratio F_0/F_1 was measured. The initial value of this ratio gives σ_{20}/σ_{21}; from this ratio and the sum $(\sigma_{20}+\sigma_{21})$ the individual cross sections may be deduced without the necessity of an analytical curve fitting. Similar experiments on the attenuation of a He^0 beam and the initial growth of He^+ and He^{++} from He^0 make it possible to estimate σ_{01} and σ_{02}.

V. EXPERIMENTAL RESULTS ON HYDROGEN IONIC AND ATOMIC BEAMS

A. Hydrogen Beams Traversing Gases

Stier and Barnett (St 56) have presented an extensive summary of the charge-changing data on hydrogen beams as of approximately May 1956 and the present review adds little in the way of new results to their report. Their results were presented in graphical form, with velocity as the independent variable. In the present review the data are tabulated, in terms of kinetic energies, and since there are a large number of graphs in Stier and Barnett's report, only the results in hydrogen are graphed here. It is, of course, true that particle velocity, rather than energy, is more fundamental to the understanding of the charge-changing process, but the kinetic energy in electron kilovolts is a number much easier to correlate with experimental equipment and with other fields of physics.

(1) *Equilibrium Charge Fractions in Gases*

Tables V-1 to V-7 present equilibrium fractions for a hydrogen beam in various gases. The equilibrium ratios at kinetic energies between 3 and 1000 kev listed in Tables V-1 to V-6 are essentially those of Stier and Barnett (St 56) and Barnett and Reynolds (Ba 58).

Other scattered values are available from the work of Bartels (Ba 32) and Ribe (Ri 51). These have been previously presented in Table III-17 of reference (Al 53) and are not repeated here. They are not in serious disagreement in that in general they lie within 10% of the values quoted here.

Above 20 kev kinetic energy, the equilibrium fractions appear to be the same, within experimental error, in nitrogen and oxygen, and hence it can be anticipated that the data for nitrogen will be applicable to air. Below 20 kev there are small but apparently real differences; the proton fraction $F_{1\infty}$ being large in nitrogen, and the H^- fraction $F_{\bar{1}\infty}$ tending to remain larger in O_2 as the energy decreases.

Table V-7, taken from Fogel and Mitin (Fo 56) gives values of the ratio $F_{\bar{1}\infty}/F_{1\infty}$ in various gases. There do not appear to be serious discrepancies between these values and those computed from Tables V-1 to V-6, considering the difficulty of obtaining high precision in this field.

TABLE V-1. Equilibrium fractions for a hydrogen beam in hydrogen gas.

Kinetic energy (kev)	$F_{\bar{1}\infty}$	$F_{0\infty}$	$F_{0\infty}$	$F_{1\infty}$
			$5+\log_{10}F_{0\infty}$	
3	0.008	0.897	···	0.095
4	0.010	0.895	···	0.095
5	0.014	0.891	···	0.095
7	0.019	0.886	···	0.095
9	0.020	0.885	···	0.095
11	0.020	0.880	···	0.100
13	0.020	0.875	···	0.105
15	0.020	0.855	···	0.125
20	0.018	0.797	···	0.185
25	0.016	0.764	···	0.220
30	0.014	0.706	···	0.280
35		0.680	···	0.320
40		0.620	···	0.380
45		0.580	···	0.420
50		0.525	···	0.475
60		0.447	4.650	0.553
70		0.361	4.556	0.639
80		0.276	4.441	0.724
90		0.237	4.375	0.763
100		0.183	4.262	0.817
150		0.063	3.800	0.937
200		0.024	3.378	0.976
250		0.075	2.874	0.993
300		0.0041	2.611	0.996
350		0.0024	2.387	0.998
400		0.0012	2.090	0.999
450		0.0_357	1.757	···
500		0.0_339	1.588	···
600		0.0_316	1.219	···
700		0.0_496	0.980	···
800		0.0_454	0.735	···
900		0.0_440	0.608	···
1000		0.0_427	0.437	···

TABLE V-2. Equilibrium fractions for a hydrogen beam in helium gas.

Kinetic energy (kev)	$F_{\bar{1}\infty}$	$F_{0\infty}$	$F_{0\infty}$	$F_{1\infty}$
			$5+\log_{10}F_{0\infty}$	
4		0.125	···	0.875
5		0.185	···	0.815
7		0.280	···	0.720
9		0.400	···	0.600
11	0.003	0.450	···	0.547
13	0.007	0.530	···	0.463
15	0.008	0.550	···	0.442
20	0.009	0.600	···	0.391
25	0.009	0.600	···	0.391
30	0.010	0.599	···	0.391
35		0.575	···	0.425
40		0.535	···	0.465
45		0.515	···	0.485
50		0.490	···	0.510
60		0.447	4.650	0.553
70		0.369	4.567	0.631
80		0.329	4.517	0.671
90		0.292	4.465	0.708
100		0.254	4.048	0.746
150		0.118	4.072	0.882
200		0.060	3.774	0.940
250		0.032	3.500	0.968
300		0.017	3.236	0.983
350		0.011	3.025	0.989
400		0.0064	2.810	0.994
450		0.0038	2.579	0.996
500		0.0028	2.443	0.997
600		0.0014	2.125	0.999
700		0.0_392	1.965	···
800		0.0_352	1.711	···
900		0.0_345	1.642	···
1000		0.0_336	1.555	···

TABLE V-3. Equilibrium fractions for a hydrogen beam in nitrogen gas.

Kinetic energy (kev)	$F_{\bar{1}\infty}$	$F_{0\infty}$		$F_{1\infty}$
		$F_{0\infty}$	$5+\log_{10}F_{0\infty}$	
4	0.004	0.871	···	0.125
5	0.006	0.854	···	0.140
7	0.011	0.815	···	0.175
9	0.012	0.778	···	0.210
11	0.014	0.756	···	0.230
13	0.013	0.712	···	0.275
15	0.012	0.688	···	0.300
20	0.010	0.640	···	0.350
25	0.008	0.587	···	0.405
30	0.006	0.544	···	0.450
35		0.500	···	0.500
40		0.480	···	0.520
45		0.430	···	0.560
50		0.410	···	0.590
60		0.384	4.562	0.616
70		0.314	4.474	0.686
80		0.240	4.358	0.760
90		0.208	4.318	0.792
100		0.172	4.236	0.828
150		0.095	3.978	0.905
200		0.038	3.572	0.962
250		0.019	3.276	0.981
300		0.010	3.106	0.990
350		0.0057	2.754	0.994
400		0.0037	2.573	0.996
450		0.0028	2.443	0.997
500		0.0020	2.305	0.998
600		0.0012	2.058	0.999
700		0.0_377	1.886	···
800		0.0_350	1.700	···
900		0.0_339	1.592	···
1000		0.0_328	1.456	···

TABLE V-4. Equilibrium fractions for a hydrogen beam in oxygen gas.

Kinetic energy (kev)	$F_{\bar{1}\infty}$	$F_{0\infty}$		$F_{1\infty}$
		$F_{0\infty}$	$5+\log_{10}F_{0\infty}$	
3	0.015	0.880	···	0.105
4	0.016	0.849	···	0.135
5	0.018	0.827	···	0.155
7	0.018	0.782	···	0.200
9	0.016	0.729	···	0.255
11	0.015	0.710	···	0.275
13	0.014	0.681	···	0.305
15	0.013	0.661	···	0.320
20	0.010	0.610	···	0.380
25	0.009	0.581	···	0.410
30	0.008	0.517	···	0.475
35		0.500	···	0.500
40		0.460	···	0.540
45		0.440	···	0.560
50		0.405	···	0.595
60		0.364	4.561	0.636
70		0.318	4.502	0.682
80		0.281	4.442	0.719
90		0.241	4.352	0.759
100		0.212	4.326	0.788
150		0.122	4.085	0.878
200		0.051	3.706	0.942

TABLE V-5. Equilibrium fractions for a hydrogen beam in neon gas.

Kinetic energy (kev)	$F_{\bar{1}\infty}$	$F_{0\infty}$		$F_{1\infty}$
		$F_{0\infty}$	$5+\log_{10}F_{0\infty}$	
4	0.0085	0.642	···	0.350
5	0.0013	0.687	···	0.300
7	0.020	0.710	···	0.270
9	0.022	0.703	···	0.285
11	0.021	0.689	···	0.290
13	0.019	0.651	···	0.330
15	0.018	0.632	···	0.350
20	0.012	0.577	···	0.415
25	0.009	0.506	···	0.485
30	0.007	0.473	···	0.520
35		0.440	···	0.560
40		0.405	···	0.595
45		0.390	···	0.610
50		0.375	···	0.625
60		0.329	4.517	0.671
70		0.298	4.474	0.702
80		0.273	4.436	0.727
90		0.239	4.378	0.761
100		0.227	4.356	0.772
150		0.130	4.114	0.870
200		0.072	3.858	0.928

TABLE V-6. Equilibrium fractions for a hydrogen beam in argon gas.

Kinetic energy (kev)	$F_{\bar{1}\infty}$	$F_{0\infty}$		$F_{1\infty}$
		$F_{0\infty}$	$5+\log_{10}F_{0\infty}$	
4	0.040	0.910	···	0.050
5	0.036	0.889	···	0.075
7	0.022	0.878	···	0.100
9	0.015	0.810	···	0.175
11	0.011	0.789	···	0.200
13	0.008	0.752	···	0.240
15	0.007	0.718	···	0.275
20	0.004	0.666	···	0.330
25	0.004	0.601	···	0.395
30	0.003	0.567	···	0.430
35		0.525	···	0.475
40		0.490	···	0.510
45		0.445	···	0.555
50		0.405	···	0.595
60		0.316	4.500	0.684
70		0.294	4.468	0.706
80		0.256	4.408	0.744
90		0.200	4.301	0.800
100		0.179	4.253	0.821
150		0.087	3.938	0.913
200		0.028	3.452	0.972
250		0.012	3.097	0.988
300		0.0054	2.732	0.996
350		0.0027	2.445	0.997
400		0.0022	2.346	0.998
450		0.0017	2.237	0.998
500		0.0014	2.162	0.999
600		0.0_397	1.988	···
700		0.0_379	1.898	···
800		0.0_361	1.786	···
900		0.0_352	1.714	···
1000		0.0_346	1.664	···

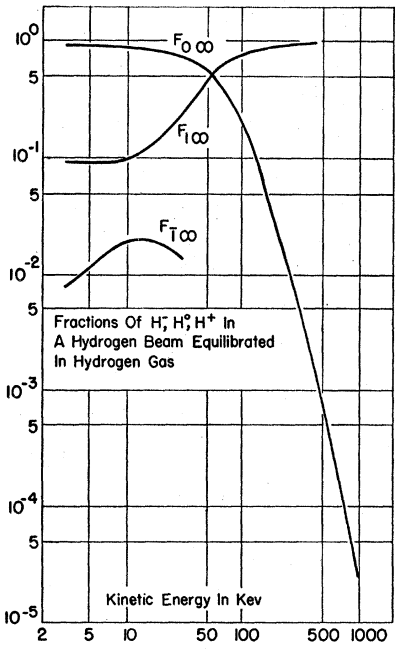

FIG. V-1. Equilibrium fractions for the components H^-, H^0, and H^+ of a hydrogen beam in hydrogen gas, at various kinetic energies.

In the case of $F_{0\infty}$, where there is a large range of variation, and the variation is rapid at high energies, linear interpolation of the tabulated values is needlessly inaccurate. The variations are more nearly linear when plotted on semilogarithmic paper (cf. Fig. V-1); therefore in some cases values of the logarithm (to the base 10) of $F_{0\infty}$ have been listed to improve the accuracy of interpolation. Thus to compute $F_{0\infty}$ for hydrogen atoms in hydrogen gas at 125 kev, interpolation by the logarithms, leading to antilog 4.030−5, or 0.107, gives a better value than the 0.123 obtained by the average of the actual ratios at 100 and 150 kev.

Figure V-1 gives a graphical summary of the equilibrium fractions of the various types of hydrogen, and of neutral hydrogen atoms, while traversing hydrogen gas.

TABLE V-7. Values of $F_{\bar{1}\infty}/F_{1\infty}$ for hydrogen beams in various gases (Fo 56).

Kinetic energy (kev)	H_2	He	N_2	O_2	Ne	A
5	0.110					
7	0.170					
9	0.185	0.020	0.045	0.035	0.062	0.049
11	0.175	0.021	0.043	0.034	0.055	0.040
13	0.145	0.022	0.037	0.031	0.043	0.027
15	0.120	0.023	0.033	0.028	0.035	0.021
20	0.087	0.023	0.021	0.018	0.020	0.013
25	0.050	0.020	0.014	0.014	0.013	0.010
30	0.040	0.016	0.011	0.010	0.010	0.0085

(2) *Measurements of Charge-Changing Collision Cross Sections*

Experimental results on the charge-changing cross sections involving H^-, H^0, H^+ are given in Tables V-8A to V-15B inclusive. In discussing the tables and the original experiments, it is convenient to consider them

TABLE V-8A. Charge-changing cross sections for H^-, H^0, H^+ in hydrogen gas. Cross sections in units of 10^{-17} cm² per atom of target hydrogen.

Kinetic energy (kev)	$\sigma_{\bar{1}0}$	$\sigma_{\bar{1}1}$	$\sigma_{0\bar{1}}$	σ_{01}	$\sigma_{1\bar{1}}$	σ_{10}	σ_{10} $22+\log_{10}\sigma_{10}$
0.2						3.8	5.580
0.4						11.0	6.041
0.6						18.0	6.255
0.8						22.5	6.352
1						26.0	6.415
2						40.0	6.602
3						44.0	6.643
4	51.0		0.64	4.20		40.0	6.602
5	51.0	1.6	0.83	4.20		40.0	6.602
7	51.0	1.8	1.10	4.20		40.2	6.604
9	52.0	2.0	1.20	4.20	0.36	40.0	6.602
11	51.0	2.0	1.20	4.60	0.42	39.8	6.600
13	49.5	2.0	1.20	5.00	0.52	38.2	6.582
15	45.8	2.1	1.10	5.40	0.62	35.8	6.554
20	42.0	2.1	0.95	6.38	0.59	29.5	6.470
25	40.2	2.1	0.81	7.28	0.40	26.0	6.415
30	38.5	2.1	0.70	8.00	0.20	21.0	6.322
35		2.1		8.00		16.0	6.204
40		2.1		8.00		14.0	6.146
45				8.00		11.0	6.041
50				7.87		9.00	5.961

TABLE V-8B. Certain charge-changing cross sections for H^-, H^0, H^+, in hydrogen gas. Cross sections in units of 10^{-17} cm² per atom of target hydrogen.

Kinetic energy (kev)	$\sigma_{\bar{1}0}$	σ_{01}	σ_{10}	σ_{10} $22+\log_{10}\sigma_{10}$
50		7.87	9.00	5.961
60		7.37	5.94	5.774
70		6.90	3.90	5.591
80		6.50	2.60	5.415
90		6.11	1.90	5.279
100		5.80	1.30	5.114
150		4.30	0.290	4.462
200		3.60	0.088	3.945
250		2.92	0.022	3.342
300		2.45	0.010	3.000
350		2.05	0.0050	2.699
400	8.5	1.99	0.0024	2.389
450		1.75	0.0010	2.000
500		1.60	0.0_362	1.792
600	6.7	1.45	0.0_324	1.380
700		1.15	0.0_311	1.041
800	5.2	1.05	0.0_457	0.756
900		0.95	0.0_438	0.586
1000	4.5	0.95	0.0_426	0.415
1200	3.78	...	...	...
1400	3.27	...	...	...

by regions of kinetic energy, rather than table by table. The lowest kinetic energy covered in this report is 0.2 kev.

Energy region 0.2–4.0 kev.—The values of $\sigma_{\bar{1}0}$ for H^- moving in the noble gases are due to Hasted (Ha 52, 55) who used the method of collecting excess negative ions. The listed values of σ_{10} in this energy range are also due to Hasted, who made measurements of the capture of an electron by a moving proton in H_2 and the noble gases. Other measurements of σ_{10} in this region have been reported by Wolf (Wo 36, 36a, 37, 37a), Goldmann (Go 31), Keene (Ke 49), and Smith (Sm 34). Smith's results in this energy range are essentially in accord with those tabulated here. These early results are displayed graphically in Fig. 231, p. 526 of Massey and Burhop (Ma 52). The results of Kasner and Donahue (Ka 57), shown in Table V-15, also extend into this energy region, but their cross sections are considerably lower than those of other observers.

Energy region 3 to 200 kev.—The tables display two sets of data on $\sigma_{\bar{1}0}$. As indicated in the tables for the target gases He, Ne, A, Kr, Xe, the combined researches of Hasted and Stedeford (Ha 55, St 55) have covered the range 0.2 to 40 kev for this quantity. The results of Stier and Barnett (St 56), lying in general in the range 3 to 35 kev are also given. The two sets of data are not, in general, in satisfactory agreement, since differences as high as 50% may be found. The methods of measurement were different; Hasted and Stedeford

TABLE V-9A. Charge-changing cross sections for H^-, H^0, H^+ in helium gas. Cross sections in units of 10^{-17} cm² per atom of helium.

Kinetic energy (kev)	$\sigma_{\bar{1}0}$ (Ha 52) (St 55)	$\sigma_{\bar{1}0}$ (St 56)	$\sigma_{\bar{1}1}$	$\sigma_{0\bar{1}}$	σ_{01}	$\sigma_{1\bar{1}}$	σ_{10}	σ_{10} $22+\log_{10}\sigma_{10}$
0.2	26						0.24	4.380
0.4	30						0.22	4.305
0.6	34						0.25	4.380
0.8	36						0.30	4.477
1	37						0.50	4.699
2	40						1.00	5.000
3	45						1.50	5.176
4	50	57.0			11.5		1.95	5.290
5	55	56.0	4.50		13.3		2.60	5.415
7	65	55.5	4.50		15.0		5.60	5.748
9	72	51.0	4.50	0.32	15.0	0.13	8.00	5.906
11	75	50.5	4.40	0.56	15.0	0.13	10.5	6.021
13	70	49.5	4.30	0.60	15.0	0.14	14.0	6.158
15	68	48.5	4.20	0.62	14.0	0.14	17.5	6.243
20	58	44.5	3.50	0.68	13.5	0.12	19.2	6.283
25	50	41.0	3.20	0.67	13.0	0.12	19.5	6.290
30	48		3.00	0.60	13.0	0.10	19.0	6.279
35			2.70		12.6		17.5	6.243
40			2.50		12.4		16.0	6.204
45					12.4		14.5	6.161
50					12.3		11.8	6.072

TABLE V-9B. Certain charge-changing cross sections for H^-, H^0, H^+ in helium gas. Cross sections in units of 10^{-17} cm² per atom of target helium.

Kinetic energy (kev)	σ_{01}	σ_{10}	σ_{10} $22+\log_{10}\sigma_{10}$
50	12.3	11.8	6.072
60	12.0	9.70	5.987
70	10.8	6.30	5.799
80	10.0	4.90	5.690
90	9.20	3.80	5.580
100	8.80	3.00	5.477
150	6.95	0.930	4.968
200	5.65	0.360	4.556
250	4.90	0.160	4.204
300	4.00	0.070	3.845
350	3.55	0.038	3.580
400	3.10	0.020	3.301
450	2.90	0.011	3.041
500	2.45	0.0068	2.832
600	2.20	0.0030	2.477
700	1.95	0.0018	2.255
800	1.65	0.0_385	1.929
900	1.50	0.0_368	1.832
1000	1.41	0.0_352	1.716

TABLE V-10. Charge-changing cross sections for H^0, H^-, H^+ in nitrogen gas. Cross sections are in units of 10^{-17} cm² per atom of nitrogen.

Kinetic energy (kev)	$\sigma_{\bar{1}0}$	$\sigma_{\bar{1}1}$	$\sigma_{0\bar{1}}$	σ_{01}	$\sigma_{1\bar{1}}$	σ_{10}	σ_{10} $22+\log_{10}\sigma_{10}$
4	88.0		0.52	10.0		59.0	
5	90.0	5.40	0.80	11.5		58.0	
7	88.0	5.45	1.20	14.5		55.0	
9	81.0	5.47	1.50	16.5	0.34	58.0	
11	78.0	5.50	1.60	16.5	0.32	50.0	
13	74.0	5.55	1.60	18.2	0.31	48.3	
15	70.0	5.62	1.45	19.0	0.29	43.0	
20	68.0	6.00	1.10	20.5	0.27	39.5	
25	68.0	6.87	0.92	21.5	0.20	34.5	
30	66.0	7.50	0.75	22.5	0.13	28.5	
35		8.25		23.0		25.5	
40		8.75		23.5		22.5	
45				24.0		19.5	
50				24.5		17.7	
60				24.0		15.0	6.176
70				24.0		11.0	6.041
80				24.0		7.6	5.881
90				24.0		6.3	5.799
100				24.0		5.0	5.699
150				21.0		2.2	5.342
200				19.3		0.75	4.875
250				17.7		0.34	4.532
300				15.0		0.16	4.204
350				14.0		0.080	3.903
400				13.3		0.050	3.699
450				11.5		0.032	3.505
500				10.0		0.020	3.010
600				9.60		0.011	3.041
700				8.70		0.0067	2.826
800				8.00		0.0040	2.602
900				7.70		0.0030	2.477
1000				7.00		0.0020	2.301

depending on ion collection, and Stier and Barnett on beam attenuation and on equilibrium measurements. The values of the equilibrium fractions $F_{\bar{1}\infty}$ given in Tables V-1 to V-7 follow more closely the results of Stier and Barnett than those of Hasted and Stedeford.

In addition to their values of $\sigma_{\bar{1}0}$ just mentioned, the values of $\sigma_{0\bar{1}}$, σ_{01}, σ_{10} in this energy region are essentially those of Stier and Barnett (St 56).

In the energy region approximately 50 to 200 kev, Montague (Mo 51) and Kanner (Ka 51) have measured σ_{01} in hydrogen, and both σ_{01} and σ_{10} in air, respectively. Their results have been reported in Allison and Warshaw (Al 53) and will not be separately reported here. In general, they are about 10% lower than those in the present tables if the air results are compared with those in nitrogen.

Ribe (Ri 51) measured σ_{10} in hydrogen gas from 25 to 150 kev, and again the results run slightly below Stier and Barnett. In the measurements of Montague, Ribe, and Kanner the attenuation of the beam in a magnetic field was measured.

Fogel *et al.* (Fo 55) have measured σ_{10} for protons in hydrogen gas, by the method of collecting excess slow positive ions. Their results were expressed in terms of the cross section per molecule of H_2; when expressed per atom they are in good agreement with those tabulated here. The range of energies covered was 12.3 to 36.7 kev.

Measurements of σ_{10} for this energy range in various gases have also been reported by Goldmann (Go 31), Keene (Ke 49), Smith (Sm 34), Bartels (Ba 30), Meyer (Me 40), and Stedeford (St 55). The measurements by Bartels and by Stedeford are in reasonable agreement with those tabulated here. Stedeford used the method of collecting excess positive charges from ionization produced in a gas. In the case of Bartels, the results were obtained by the method, applicable to a two-component system, of making a measurement of F_1 and of $F_{1\infty}$.

Whittier (Wh 54) has measured σ_{10} in hydrogen gas in the approximate range 4 to 70 kev, using the method of attenuation in a magnetic field and obtaining results which agree closely with Ribe and with Stier and Barnett. He has also measured $\sigma_{\bar{1}0}$ in this range, obtaining results which are as much as 20% higher than those tabulated, in the range 3 to 20 kev, but which agree more closely from 20 to 70 kev.

The measurements of $\sigma_{\bar{1}1}$, in the energy range 5 to 40 kev, are those of Fogel *et al.* (Fo 57). They were obtained by finding the linear and parabolic contributions to the growth of a protonic constituent from a

TABLE V-11. Charge-changing cross sections for H^0, H^-, H^+ in oxygen gas. Cross sections in units of 10^{-17} cm² per atom of oxygen.

Kinetic energy (kev)	$\sigma_{\bar{1}0}$	$\sigma_{\bar{1}1}$	$\sigma_{0\bar{1}}$	σ_{01}	$\sigma_{1\bar{1}}$	σ_{10}
4			1.0	8.50		49.0
5	50.0	4.25	1.0	9.50		47.0
7	51.4	4.30	1.1	13.5		45.0
9	52.8	4.50	1.2	14.5	0.57	43.0
11	54.2	4.55	1.2	15.5	0.56	40.0
13	55.6	4.75	1.2	16.0	0.53	37.0
15	56.0	5.00	1.1	18.8	0.50	33.0
20	58.5	6.00	0.95	19.0	0.44	29.2
25	58.7	6.25	0.82	19.3	0.35	28.0
30	59.0	6.81	0.72	19.6	0.27	23.5
35		7.50		19.8		20.0
40		8.34		20.1		18.7
45				20.2		18.2
50				20.3		14.0
60				20.3		11.6
70				20.4		9.50
80				20.5		8.00
90				20.5		6.50
100				20.5		5.50
150				19.5		2.70
200				19.0		1.03
400	34.4					
600	27.6					
800	23.5					
1000	19.1					
1250	17.6					
1500	12.6					

TABLE V-12. Charge-changing cross sections for H^-, H^0, H^+ in neon gas. Cross sections in units of 10^{-17} cm² per atom of neon.

Kinetic energy (kev)	$\sigma_{\bar{1}0}$ (Ha 52)	$\sigma_{\bar{1}0}$ (St 55)	$\sigma_{\bar{1}0}$ (St 56)	$\sigma_{\bar{1}1}$	$\sigma_{0\bar{1}}$	σ_{01}	$\sigma_{1\bar{1}}$	σ_{10}
0.2	22							~0.5
0.4	24							~0.6
0.6	25							1.2
0.8	25							2.0
1	25							3.0
2	35							8.5
3	39							13.5
4	41	34			0.44	6.7		17.5
5	45	35	3.0		0.65	8.0		20.5
7	49	39	3.5		1.30	10.5		27.0
9	52	40	4.2		1.50	11.5	0.19	29.0
11	54	41	4.8		1.50	12.0	0.18	29.5
13	57	42	5.0		1.40	15.0	0.17	29.0
15	58	44	5.1		1.30	16.5	0.12	28.0
20	60	48	5.2		1.00	17.7	0.10	23.5
25	62	49	5.3		0.85	18.5	0.08	20.0
30	62	49	5.4		0.60	18.7	0.05	19.0
35	62		5.52			19.0		16.5
40	63		5.73			19.5		14.0
45						19.7		12.0
50						20.0		11.5
60						20.0		9.80
70						20.0		8.50
80						20.0		7.50
90						19.7		6.20
100						19.5		5.75
150						18.7		2.80
200						18.0		1.40

prepared beam of 100% H^-. The cross sections, which are of the order of 4 to 10% of $\sigma_{\bar{1}0}$, seem surprisingly large. Allison (Al 58) was unable to find the double electron loss cross-section σ_{02} for helium atoms of 250 kev energy in helium, and set an upper limit for this cross section of about 2% of that for the single electron

TABLE V-13A. Charge-changing cross sections for H^-, H^0, H^+ in argon gas. Cross sections in units of 10^{-17} cm² per atom of argon.

Kinetic energy (kev)	$\sigma_{\bar{1}0}$ (Ha 52)	$\sigma_{\bar{1}0}$ (St 55)	$\sigma_{\bar{1}0}$ (St 56)	$\sigma_{\bar{1}1}$	$\sigma_{0\bar{1}}$	σ_{01}	$\sigma_{1\bar{1}}$	σ_{10}
0.2	52							20
0.4	54							38
0.6	58							62
0.8	65							95
1	68							120
2	75							140
3	85							145
4	100	80			3.7	13.0		155
5	125	88		3.75	3.5	15.5		130
7	166	105		4.50	3.0	18.0		117
9	177	120		5.90	2.5	20.5	0.39	105
11	184	135		7.20	2.2	24.0	0.38	90.0
13	190	150		7.80	1.9	26.0	0.37	83.0
15	195	160		8.75	1.4	29.0	0.36	80.0
20	205	175		11.7	1.1	33.0	0.33	71.0
25	215	180		13.2	1.1	38.0	0.31	64.0
30	224	180		15.0	1.0	40.0	0.33	59.0
35	226			16.2		43.0		50.0
40	230			17.4		45.0		44.0

TABLE V-13B. Certain charge-changing cross sections for H^0, H^+ in argon gas. Cross sections in units of 10^{-17} cm² per argon atom.

Kinetic energy (kev)	$\sigma_{\bar{1}0}$	σ_{01}	σ_{10}
40		45.0	44.0
45		46.0	38.0
50		47.5	33.0
60		47.5	22.0
70		48.0	20.0
80		48.0	16.5
90		48.0	12.0
100		45.0	9.80
150		40.0	3.80
200		37.0	1.08
250		30.0	0.380
300		28.7	0.150
350		26.5	0.074
400	61.7	22.5	0.050
450		22.0	0.038
500	52.0	20.0	0.029
600	51.0	19.5	0.019
700		19.0	0.015
800	42.9	18.0	0.011
900		17.0	0.0088
1000	41.7	16.5	0.0076
1500	36.3	...	...
1750	32.7	...	...

TABLE V-14. Certain charge-changing cross sections for H^- and H^+ in krypton and xenon gases. Cross sections in units of 10^{-17} cm² per atom of gas.

Kinetic energy (kev)	Krypton			Xenon		
	$\sigma_{\bar{1}0}$	$\sigma_{\bar{1}1}$	σ_{10}	$\sigma_{\bar{1}0}$	$\sigma_{\bar{1}1}$	σ_{10}
0.2	60		130	70		120
0.4	63		250	75		363
0.6	65		266	79		366
0.8	72		264	86		356
1	80		260	93		343
2	92		240	105		290
3	100		228	125		268
4	125		215	225		250
5	195	2.75	197	285		239
7	267	4.50	170	337		199
9	283	7.70	150	354		185
11	295	10.0	138	364	7.5	170
13	300	11.0	129	374	9.5	155
15	305	12.0	116	376	11.9	135
20	313	12.2	100	390	12.7	125
25	317	12.5	88	400	15.0	108
30	324	12.5	75	410	16.1	90
35	326	12.6	69	414	17.0	75
40	336	12.65	64	422	17.6	60

TABLE V-15A. Charge-changing cross sections for H^+ ions in hydrogen gas. Cross sections in units of 10^{-17} cm² per atom of target hydrogen (Ka 57).

Kinetic energy (kev)	σ_{10}
2	(22.9)[a]
3	26.4
4	29.1
7	34.3
9	35.8
11	35.3
13	34.1
15	32.3
20	27.7
25	22.5
30	17.6
35	(12.5)[a]

[a] Extrapolated.

TABLE V-15B. Charge-changing cross sections $\sigma_{\bar{1}0}$ for H^- ions in CO_2 gas. Cross sections in units of 10^{-17} cm² per molecule of CO_2 (Ro 58).

Kinetic energy (kev)	$\sigma_{\bar{1}0}$
400	82.5
500	74.0
600	61.7
800	54.5
1000	52.1
1500	44.0
1750	39.7

TABLE V-16. Coefficients $P(z,i)$ and $N(z,i)$ for the three-component system H^-, H^0, H^+ [cf. Eq. (II-12)].
$q=+\frac{1}{2}[(g-a)^2+4bf]^{\frac{1}{2}}$; $s=\frac{1}{2}(g-a)$; $a=-(\sigma_{0\bar{1}}+\sigma_{01}+\sigma_{10})$; $b=\sigma_{\bar{1}0}-\sigma_{10}$; $f=\sigma_{0\bar{1}}-\sigma_{1\bar{1}}$; $g=-(\sigma_{\bar{1}0}+\sigma_{\bar{1}1}+\sigma_{1\bar{1}})$.

Original state at $\pi=0$	$P(z,i)$	$N(z,i)$
(A) To calculate changes in the fraction of H^0 present in a beam in which originally all the ions had the same charge.		
All H^-	$P(\bar{1},0)=\frac{1}{2q}[bF_{1\infty}+(b+s-q)F_{0\infty}]$	$N(\bar{1},0)=-\frac{1}{2q}[bF_{1\infty}+(b+s+q)F_{0\infty}]$
All H^0	$P(0,0)=-\frac{1}{2q}[(s-q)(1-F_{0\infty})+bF_{\bar{1}\infty}]$	$N(0,0)=\frac{1}{2q}[(s+q)(1-F_{0\infty})+bF_{\bar{1}\infty}]$
All H^+	$P(1,0)=\frac{1}{2q}[F_{0\infty}(s-q)-bF_{\bar{1}\infty}]$	$N(1,0)=-\frac{1}{2q}[F_{0\infty}(s+q)-bF_{\bar{1}\infty}]$
(B) To calculate changes in the fraction of H^- present in a beam in which originally all the ions had the same charge.		
$z\|e\|$	$P(z,\bar{1})=P(z,0)(s+q)/b$ $z=\bar{1}, 0, 1$	$N(z,\bar{1})=N(z,0)(s-q)/b$ $z=\bar{1}, 0, 1$
(C) To calculate changes in the fraction of H^+ present in a beam in which originally all the ions had the same charge.		
$z\|e\|$	$P(z,1)=-P(z,0)(b+s+q)/b$ $z=\bar{1}, 0, 1$	$N(z,1)=-N(z,0)(b+s-q)/b$ $z=\bar{1}, 0, 1$

loss, σ_{01}. A remarkable feature of the measurements of Fogel *et al.* is that whereas collisions of 40 kev H^- ions with argon and xenon atoms have roughly the same probability for simultaneous loss of both electrons from H^-, collisions with krypton are only 70% as effective in this respect.

The tabulated values of $\sigma_{1\bar{1}}$ for protons in H_2, He, N_2, O_2, Ne, and A are from Fogel and Mitin (Fo 56) by the method of observing the initial rate of growth of H^- from a beam of pure protons.

In Table V-15 are given some measurements of σ_{10} for protons in hydrogen gas by Kasner and Donahue (Ka 57). These results, obtained by the method of collection of the excess slow positive ions, are not in agreement with those of other observers, being lower. They run from approximately 55% of the values listed in Table V-8A at 2 kev, to 78% at 35 kev. The explanation of this discrepancy is not yet at hand.

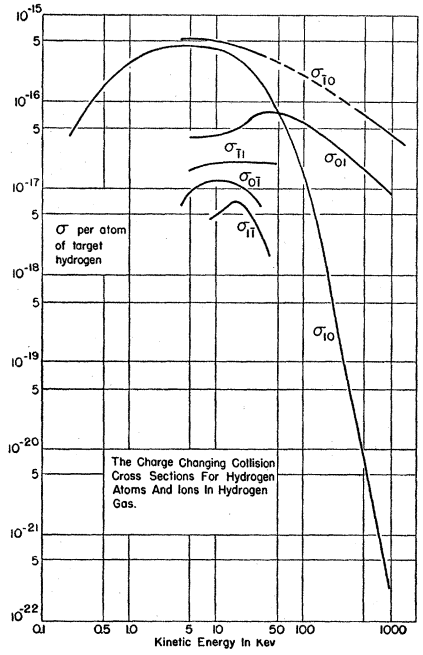

FIG. V-2. The charge-changing cross sections for H^-, H^0, and H^+ ions and atoms moving in hydrogen gas.

Energy region 200 to 1750 kev.—The measurements of σ_{01} and σ_{10} in this region are due to Barnett and Reynolds (Ba 58). The cross-section σ_{01} was measured by the attenuation of a neutral beam in a transverse electric field. The equilibrium fractions $F_{1\infty}$ and $F_{0\infty}$ were then measured and σ_{10} computed from Eqs. (II-33) and (II-34).

The tables also contain values of $\sigma_{\bar{1}0}$ at energies above 400 kev, due to Rose *et al.* (Ro 58). The negative hydrogen ions were obtained directly from an ion source and accelerated in the first stage of a tandem Van de Graaff. Data were taken in H_2, O_2, A, and CO_2 gases. The results in CO_2 are given separately in Table V-15A.

In order to visualize the trend of the variation of the various hydrogen beam cross sections with energy, the

TABLE V-17. Quantities for computing hydrogen beam compositions in the three-component system H^-, H^0, H^+ [cf. Eq. (II-12)].

Kinetic energy (kev)	$F_{\bar{1}\infty}$	$F_{0\infty}$	$F_{1\infty}$	$10^{17}q$	$\frac{1}{2}\Sigma\sigma_{if}\times10^{17}$
		Hydrogen			
9	0.020	0.887	0.093	5.49	49.9
15	0.021	0.852	0.128	3.80	45.4
25	0.016	0.790	0.193	3.30	40.1
		Nitrogen			
9	0.008	0.773	0.219	7.12	81.2
15	0.014	0.684	0.302	8.37	72.3
25	0.008	0.611	0.380	9.82	66.0
		Neon			
9	0.024	0.681	0.294	3.86	43.7
15	0.017	0.618	0.365	4.67	47.5
25	0.010	0.515	0.475	8.10	46.9

TABLE V-18A. Numerical values of the coefficients $P(z,i)$ for computing the composition of the three-component charge system H^-, H^0, H^+.

Kinetic energy (kev)	$P(\bar{1},\bar{1})$	$P(\bar{1},0)$	$P(\bar{1},1)$	$P(0,\bar{1})$	$P(0,0)$	$P(0,1)$	$P(1,\bar{1})$	$P(1,0)$	$P(1,1)$
					Hydrogen				
9	0.022	0.266	−0.288	0.007	0.081	−0.088	0.070	0.827	−0.897
15	0.036	0.514	−0.549	0.001	0.108	−0.115	0.055	0.801	−0.857
25	0.063	0.893	−0.956	0.011	0.159	−0.170	0.051	0.727	−0.778
					Nitrogen				
9	0.062	0.914	−0.977	0.013	0.189	−0.202	0.048	0.702	−0.749
15	0.079	0.993	−1.072	0.020	0.253	−0.273	0.049	0.619	−0.668
25	0.025	1.103	−1.128	0.008	0.360	−0.368	0.013	0.602	−0.616
					Neon				
9	0.460	1.112	−1.572	0.040	0.097	−0.364	0.130	0.313	−0.443
15	0.235	1.261	−1.494	0.043	0.232	−0.275	0.083	0.451	−0.534
25	0.069	1.307	−1.376	0.022	0.422	−0.444	0.025	0.484	−0.509

TABLE V-18B. Numerical values of the coefficients $N(z,i)$ for computing the composition of the three-component charge system H^-, H^0, H^+.

Kinetic energy (kev)	$N(\bar{1},\bar{1})$	$N(\bar{1},0)$	$N(\bar{1},1)$	$N(0,\bar{1})$	$N(0,0)$	$N(0,1)$	$N(1,\bar{1})$	$N(1,0)$	$N(1,1)$
					Hydrogen				
9	0.958	−1.152	0.195	−0.027	0.032	−0.005	−0.090	−1.714	1.803
15	0.944	−1.365	0.422	−0.022	0.041	−0.012	−0.076	−1.653	1.729
25	0.921	−1.683	0.762	−0.028	0.051	−0.023	−0.068	−1.517	1.584
					Nitrogen				
9	0.924	−1.688	0.758	−0.021	0.038	−0.017	−0.056	−1.474	1.530
15	0.907	−1.677	0.770	−0.034	0.063	−0.029	−0.063	−1.304	1.366
25	0.967	−1.715	0.747	−0.016	0.019	−0.012	−0.022	−1.214	1.235
					Neon				
9	0.516	−1.793	1.277	−0.064	0.222	−0.159	−0.154	−0.994	1.148
15	0.750	−1.880	1.128	−0.060	0.150	−0.090	−0.100	−1.069	1.169
25	0.922	−1.822	0.901	−0.032	0.063	−0.031	−0.035	−0.998	1.034

results in hydrogen gas are graphically displayed in Fig. V-2. The gross features of the behavior shown in Fig. V-2 are typical of all gases, with certain interesting exceptions at low kinetic energies. For instance, in the region below 15 kev the cross-section σ_{10} in helium falls off very sharply as the energy decreases, due to the difficulty experienced by the proton in dislodging and capturing one of the tightly bound helium electrons.

(3) *Stages in the Charge Equilibration of Hydrogen Beams*

If the individual cross sections for charge-changing collisions are known, the growth of new charge states in a prepared pure ionic or atomic beam may be calculated by Eq. (II-12). The interpretation of the quantities in this equation for the case of the H^-, H^0, H^+ system is given in Table V-16. There is considerable interest in the growth of H^- due to its practical application in the operation of tandem Van de Graaff accelerators. The largest value of $F_{I\infty}$ apparently occurs in hydrogen gas, at approximately 15 kev kinetic energy. Table V-17 lists numerical values of the quantities in Eq. (II-12) which do not depend on the initial conditions, and are useful in computing the growth of H^- from an initial H^+ beam. There are small discrepancies between the values of $F_{i\infty}$ collected in Table V-17 and those previously presented in Tables V-1, V-3, and V-5. This is due to the fact that the values in Table V-17 are calculated directly from the individual cross sections, as given in Tables V-8A, V-10, and V-12 using equations such as (II-23). The largest discrepancy is in $F_{1\infty}$ for hydrogen gas at 25 kev; the value calculated from the cross sections is lower by 12% than that given in Table V-1.

Table V-18 lists numerical values of $P(z,i)$ and $N(z,i)$ computed according to the directions of Table V-16 and applicable to the computation of the changing charge composition of a beam which is originally either all H^-, H^0, or H^+.

As an example of computations from Tables V-16,

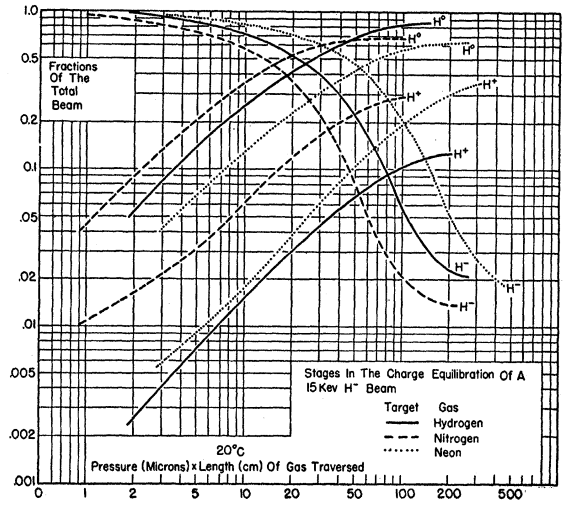

FIG. V-3. Growth of H^0 and H^+, and decay of H^- in an originally pure H^- beam as it traverses the gases hydrogen, nitrogen, or neon (15 kev).

V-17, and V-18, Figs. V-3 and V-4 show the process of charge equilibration of H^- and H^+ beams of 15 kev kinetic energy as they traverse increasing amounts of the target gases H_2, N_2, and Ne. Instead of plotting the fractions F_i against π, the number of atoms of gas/cm^2 traversed, the independent variable (pl) is used where p is the gas pressure in microns at 20°C and l is the length of path of the hydrogen beam in the gas. At 20°C the relations between (pl) and π are

$$\text{monatomic gas} \quad \pi=3.30\times10^{13}(pl),$$
$$\text{diatomic gas} \quad \pi=6.61\times10^{13}(pl).$$

From Fig. V-4, we see that the maximum conversion of H^+ to H^- at 15 kev, in a collision chamber 10 cm long

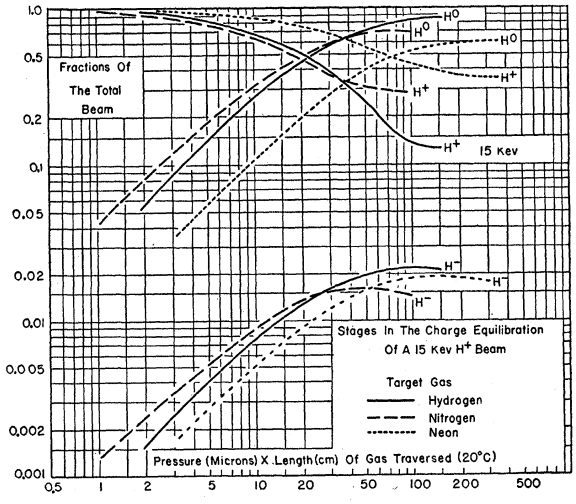

FIG. V-4. Growth of H^- and H^0, and decay of H^+ in an originally pure H^+ beam as it traverses the gases hydrogen, nitrogen, or neon (20°C).

containing H_2 gas takes place at approximately 10 microns pressure.

(4) *Charge-Changing Cycles in the Moderation of Fast Protons*

Some aspects of the charge-changing phenomena which take place in the slowing down of protons are shown in Figs. V-5 and V-6. Figure V-5 is a plot, for protons in H_2, He, and N_2 target gases of the derivative dN_c/dE of Eq. (III-4), where σ_c is defined in Eq. (III-3). The values of dE/dx, the stopping power of the gases for hydrogen beams, were taken from the recent compilation by Whaling (Wh 57). In helium gas, the loss of 1 kev kinetic energy by a 12-kev hydrogen beam is accompanied by 17.6 charge-changing cycles, in each of which an electron is captured and lost. Figure V-6 concerns the fraction of the time spent as a neutral atom by a proton slowing down in H_2 or N_2 target gas. The curves labeled "total" are computed from

$$dt/dE=\frac{p_0T}{pT_0}\frac{1}{\epsilon(E)V(E)}, \qquad \text{(V-1)}$$

where p_0, T_0 are 76 cm Hg and 273°K, respectively; $\epsilon(E)$ is the stopping power of the gas in kev per cm at p_0, T_0; $V(E)$ is the speed of the beam particles in cm/sec; and dt/dE is the time required to lose one kev of energy from all causes, at p, T, which are considered to be 76 cm and 293°K.

The "neutral" curves of Fig. V-6 are plots of the derivative dt_c/dE of Eq. (III-5) and show the time spent as a neutral atom during the period in which one kev kinetic energy is lost at 20°C and 1 atmos pressure.

The curves of Figs. V-5 and V-6 may be applied to tritons, deuterons, positive mesons, or hyperons by multiplying the kinetic energy as given along the axis of abscissas by the ratio of the mass of the particle to that of the proton. Thus, from Fig. V-5 the maximum number of capture and loss cycles per unit energy loss for a μ^+ meson in helium gas occurs at 1.4 kev kinetic energy, and has the value 17.6 cy per kilovolt energy loss.

Table V-19 shows some results of numerical integration of Eqs. (III-4) and (III-5). The total number of capture and loss cycles in the slowing down of a fast proton is finite, since at kinetic energies more than several hundred kilovolts the cycles cannot begin because the fast protons cannot capture an electron, and at energies less than a kilovolt, a noncyclic condition is again reached as the particle approaches the equipartition energy in the gas. One may legitimately raise the question as to whether the 680 charge-changing cycles specified for the slowing down of a proton in hydrogen is a number which is independent of the gas pressure. Bohr (Bo 48) has interpreted some of the experiments of Lassen (La 55) on the effective

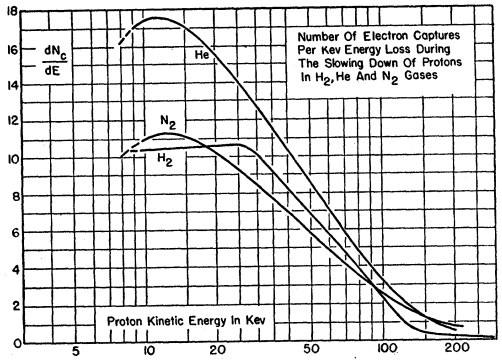

FIG. V-5. The number of capture and loss cycles in a hydrogen beam during the loss of 1 kev kinetic energy, due to all causes, as determined by stopping power measurements.

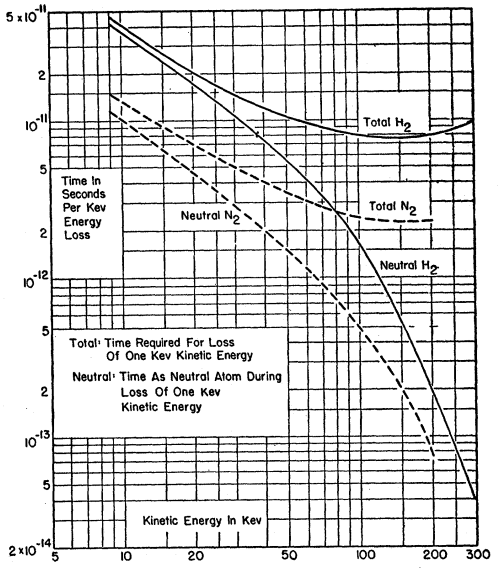

FIG. V-6. Time scales for the moderation of fast protons in hydrogen or nitrogen gas at 76 cm pressure, 293°K. For total time in the neutral condition see Table V-19.

charge of moderating fission fragments as a function of gas pressure by assuming a pressure effect on the electron loss cross sections, due to the fact that at high gas pressures the time interval between collisions is so short that ionization of the moving fission fragment from a metastable state is possible. The absence of metastable levels in hydrogen which are located sufficiently below those from which there are allowed transitions to the ground state mitigates against such a pressure effect for protons, but rigorous experimental evidence of the absence of such an effect in the effective charge of a proton beam is lacking.

The time spent as a neutral in slowing down in a gas is, of course, inversely proportional to the pressure, and the estimates in the table are for one atmosphere pressure at 20°C.

Some rough values for the number of cycles in which negative ions are formed are included in Table V-19. In the target gases H_2 and N_2 negative ions isotopic with H^- are formed essentially through electron capture by the neutral moving ion, which is the dominant constituent of the beam at the energies where the negative ion is formed in appreciable amounts.

The cross section $\sigma_{\bar{1}0}$ is very large compared to $\sigma_{0\bar{1}}$, so that for the $0\rightleftarrows\bar{1}$ cy, $\sigma_c \doteq \sigma_{0\bar{1}}$ [cf. Eq. (III-3)]. The cycle can be considered as originating from the neutral constituent alone, and the diminution in F_0 neglected.

In the target gas helium, where H^- is less readily produced than in H_2 or N_2, the situation is not so simple. At the lower energies of Table V-2 it is seen that, since the slow moving proton cannot capture one of the tightly bound electrons of helium, $F_1 > F_0$, contrary to the situation in H_2 and N_2. Furthermore the cross sections of Table V-9A indicate that $\sigma_{0\bar{1}}$ is only 3 to 5 times larger than $\sigma_{1\bar{1}}$. Thus the production of H^- from H^+, proportional to $F_1\sigma_{1\bar{1}}$, is not negligible compared to production from H^0, proportional to $F_0\sigma_{0\bar{1}}$. Table V-19 gives an estimate only of the number of cycles $0\rightleftarrows\bar{1}$.

(5) *Minimum Energy Loss due to Charge Changing*

Since, as we have seen in Sec. III-D, each cycle is accompanied by the creation of one ion pair from the

TABLE V-19. Data concerning charge-changing events in the slowing down of protons, deuterons, and μ^+ mesons.

Event	Gas	Proton $E_0>300$ kev $E_f=$ 9 kev	Deuteron $E_0>600$ kev $E_f=$ 18 kev	μ^+ meson $E_0>35$ kev $E_f=$ 1 kev
No. of charge-changing cycles $0\rightleftarrows1$ during moderation in	H_2	680	1260	80
	He	980	1960	115
	N_2	660	1320	77
No. of charge-changing cycles $0\rightleftarrows\bar{1}$ during moderation in	H_2	$\gtrsim$50	$\gtrsim$100	$\gtrsim$6
	He	$\gtrsim\gtrsim$16[a]	$\gtrsim\gtrsim$32[a]	$\gtrsim\gtrsim$2[a]
	N_2	$\gtrsim$15	$\gtrsim$30	$\gtrsim$2
Time spent as a neutral particle during moderation at 76 cm pressure in	H_2	11×10^{-10} sec	22×10^{-10} sec	1.3×10^{-10} sec
	He	12	24	1.3
	N_2	2.4	4.8	0.3

[a] See comment in text.

TABLE V-20A. Charge distribution in hydrogen beams emerging from solid foils.

Kinetic energy (kev)	Beryllium			Aluminum			"Old surfaces"			Be, Al, Ag (Ha 50)		
	$F_{\bar{1}\infty}$	$F_{0\infty}$	$F_{1\infty}$	$F_{\bar{1}\infty}$	$F_{0\infty}$	$F_{1\infty}$	$F_{\bar{1}\infty}$	$F_{0\infty}$	$F_{1\infty}$	$F_{\bar{1}\infty}$	$F_{0\infty}$	$F_{1\infty}$
4	···	···	···	0.062	0.856	0.082	0.045	0.810	0.145			
7	0.035	0.828	0.137	0.048	0.840	0.112	0.030	0.773	0.197			
10	0.031	0.793	0.176	0.040	0.818	0.142	0.023	0.727	0.250			
20	0.019	0.671	0.310	0.024	0.725	0.251	0.012	0.612	0.376			
25	0.014	0.611	0.375	0.017	0.643	0.340	0.011	0.56	0.430	···	0.44	0.56
50	0.003	0.341	0.656	0.0037	0.356	0.640	0.005	0.425	0.570	···	0.32	0.68
75	0.015	0.195	0.790	0.0015	0.20	0.80	0.004	0.30	0.70	···	0.28	0.72
100	···	0.134	0.866	0.0_36	0.120	0.879	0.001	0.200	0.799	···	0.18	0.82
125	···	0.08	0.92	···	0.08	0.92	0.0_38	0.13	0.87	···	0.14	0.86
150	···	0.048	0.95	0.0_34	0.045	0.955	0.0_32	0.088	0.912	···	0.091	0.909
175	···	0.03	0.97	···	0.03	0.97	···	0.05	0.95	···	0.061	0.939
200	···	0.01	0.99	···	0.02	0.98	···	0.03	0.97	···	0.046	0.954
250										···	0.022	0.978
300										···	0.016	0.984
350										···	0.011	0.989
400										···	0.005	0.995

TABLE V-20B. Charge distribution in hydrogen beams emerging from solid foils.

Kinetic energy (kev)	Silicon monoxide			Calcium			Silver		
	$F_{\bar{1}\infty}$	$F_{0\infty}$	$F_{1\infty}$	$F_{\bar{1}\infty}$	$F_{0\infty}$	$F_{1\infty}$	$F_{\bar{1}\infty}$	$F_{0\infty}$	$F_{1\infty}$
7	0.029	0.771	0.200	0.024	0.801	0.175	0.029	0.771	0.200
10	0.023	0.730	0.247	0.013	0.683	0.304	0.023	0.730	0.247
20	0.013	0.619	0.368	0.005	0.462	0.533	0.117	0.682	0.301
25	···	···	···	0.003	0.41	0.59	0.014	0.67	0.350
50	0.004	0.398	0.598	0.001	0.262	0.737	0.004	0.398	0.598
75	···	···	···	···	0.17	0.83	0.001	0.27	0.730
100	0.0_36	0.160	0.839	···	0.117	0.883	0.0_37	0.184	0.815
125	···	···	···	···	0.08	0.92	···	0.13	0.87
150	0.0_34	0.076	0.924	···	0.05	0.950	0.0_32	0.088	0.912
175					0.03	0.97	···	0.07	0.93
200					0.01	0.99	···	0.05	0.95

TABLE V-20C. Charge distribution in hydrogen beams emerging from solid foils.

Kinetic energy (kev)	Gold			Gold (Ha 50)		
	$F_{\bar{1}\infty}$	$F_{0\infty}$	$F_{1\infty}$	$F_{\bar{1}\infty}$	$F_{0\infty}$	$F_{1\infty}$
4	0.042	0.856	0.102			
7	0.038	0.830	0.132			
10	0.035	0.800	0.165			
20	0.028	0.705	0.267			
25	0.023	0.637	0.340	···	0.44	0.56
50	0.004	0.401	0.595	···	0.32	0.68
75	0.002	0.27	0.73	···	0.25	0.75
100	0.0_39	0.195	0.804	···	0.20	0.80
125	···	0.16	0.840	···	0.15	0.85
150	0.0_35	0.134	0.876	···	0.11	0.89
175	···	0.10	0.90	···	0.09	0.91
200	···	0.08	0.92	···	0.06	0.94
250				···	0.03	0.97
300				···	0.016	0.984
350				···	0.012	0.988
400				···	0.010	0.990

target gas, we may set a lower limit to the contribution to the total 1 kev energy loss from charge changing in helium by using the ionization potential of helium (24.5 v), which gives 0.431 kev, or 43% of the loss as due to charge-changing events. There is strong reason to anticipate, of course, that the average energy loss to the target gas per charge-changing cycle is greater than its ionization potential, but experimental determinations of this number have apparently not been made.

In N_2 gas (ionization potential 15.5 v) the maximum fractional energy loss due to charge-changing collisions occurs at about the same hydrogen kinetic energy and by the above argument is at least 17%. In hydrogen gas, the maximum seems to be at about 25 kev and, taking the ionization potential of the molecule as 16 v, at least 17% of the total energy loss must be in the charge-changing cycles. The charge-changing cycles giving H^- are ignored here.

B. Hydrogen Beams Equilibrated in Solid Foils

A beam of protons, incident on a thin foil, is found to emerge containing in general H^-, H^0, and H^+ ions and atoms. Little can be said as to what goes on in the interior of the solid; no measurements have been attempted in solids analogous to those resulting in charge-changing collision cross sections in gases. It would be extremely difficult to prepare foils so thin that equilibrium between the various charge states would not have been set up in traversal of them. The charge equilibrium in the emergent beam is determined by the last few atomic layers, and thus it is difficult to say whether the result can be called typical of the bulk material, or should be attributed to adsorbed layers, or chemically affected layers, on the foil surface (cf. Ph 53).

Equilibria set up in solid foils have been reported by Bartels (Ba 30). The energy region he investigated has been covered by more recent experiments, and his data are not included in this review.

Hall (Ha 50) investigated the hydrogen beams emerging from Be, Al, Ag, and Au foils. He analyzed the emergent beam by the method of subtraction, that is, he allowed first the entire emergent beam to produce light in a KI(Tl) crystal, and then deviated away the charged components, obtaining a response proportional to the neutral beam alone. It was assumed that the light produced was independent of the charge composition of the hydrogen beam incident on the crystal. Thus Hall actually measured $(F_{\bar{1}\infty}+F_{1\infty})$ and $F_{0\infty}$. The vacuum in the foil chamber was not better than 10^{-6} mm Hg, thus adsorbed or oxidized layers on the foils may well have existed. Hall found the same equilibrium from foils of Be, Al, Ag (see Table V-20A) but a somewhat higher neutral fraction from gold foils (Table V-20C).

Phillips (Ph 55) has also made such measurements and extended them to measure independently the three fractions $F_{\bar{1}\infty}$, $F_{0\infty}$, and $F_{1\infty}$. He also investigated the effect of evaporating fresh emergent surfaces on the foils while in place in the vacuum. In this way he found that freshly evaporated surfaces gave equilibria different from surfaces which had been aged in vacuum; freshly evaporated Al produced an $F_{1\infty}=0.26$; after about 16 min at a pressure of 2.4×10^{-5} mm the value had risen to 0.38 (cf. Fig. V-7). All foils which had aged in the vacuum produced the same equilibria; see "old surfaces" in Table V-20A. Freshly evaporated surfaces produced equilibria characteristic of the bulk material; the uniformity found by Hall was not present.

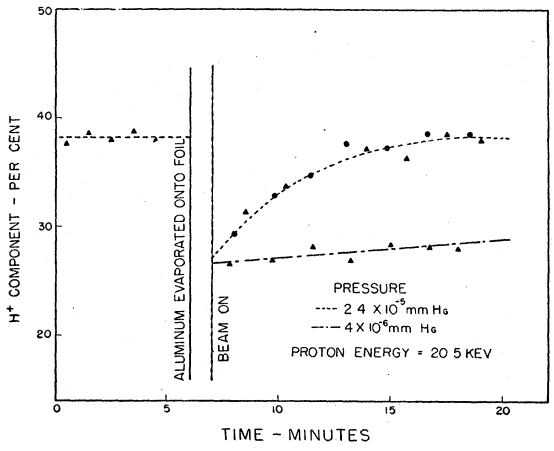

FIG. V-7. Surface aging effect on $F_{1\infty}$ in a hydrogen beam emerging from an aluminum surface (Ph 55). A fresh aluminum surface was sublimed onto the foil at approximately $t=6$ min.

TABLE V-20D. Ratio of negatives to positives in a hydrogen beam emerging from foils.

Foil material	Proton energy (kev)	$F_{\bar{1}\infty}/F_{1\infty}$
Be	27.4	0.134
	21.3	0.201
	14.3	0.323
	11.5	0.400
Al	28.2	0.060
	20.2	0.109
	15.0	0.181

The results on hydrogen beams emerging from solids are displayed in Tables V-20A, V-20B, and V-20C. The equilibria from fresh surfaces of Be, Al, Ca, Ag, Au, and Si are due to Phillips (Ph 55) and also those from "old surfaces." The results of Hall are also quoted.

The results of Hall on the charge equilibria emerging from gold do not agree with those of Phillips below 100 kev (cf. Table V-20C). Phillips finds an almost 50% larger $F_{0\infty}$ than Hall found, and gold should be a type of material least rapidly affected by surface changes. It may be of interest to note that in the measurement of stopping power of foils, the results of different observers seem least likely to agree when gold is used as noted by Whaling (Wh 57).

Fogel and his co-workers (Fo 56a) have studied the formation of negative hydrogen ions in hydrogen beams emergent from thin foils of Be, Al, and Cu. The kinetic energies of the incident protons were in the range 11.5 to 28 kev. Using incident H_2^+ beams, the emergent beam showed the same composition as from an incident proton beam of half the kinetic energy, and an incident deuteron beam was equivalent to a proton beam of twice the energy. The results from copper foils followed the aluminum results in Table V-20D quite closely. Beryllium seems a more efficient converter than Al or Cu, and in all cases the yield of negatives is larger than reported by Phillips.

VI. EXPERIMENTAL RESULTS ON HELIUM IONIC AND ATOMIC BEAMS

A. Helium Beams Traversing Gases

Considerable information concerning the charge-changing behavior of helium beams traversing gases is available in the kinetic energy range 4 to 450 kev, with

TABLE VI-1. Equilibrium fractions for a helium beam in the target gases H_2 and He.

Kinetic energy (kev)	Hydrogen gas[a]			Helium gas		
	$F_{0\infty}$	$F_{1\infty}$	$F_{2\infty}$	$F_{0\infty}$	$F_{1\infty}$	$F_{2\infty}$
8	0.849	0.151	···	0.972	0.028	···
12	0.839	0.161	···	0.955	0.045	···
16	0.834	0.166	···	0.938	0.062	···
20	0.840	0.166	···	0.925	0.075	···
40	0.825	0.175	···	0.848	0.154	0.0023
60	0.805	0.195	···	0.792	0.204	0.0039
80	0.760	0.240	···	0.747	0.248	0.0048
100	0.709	0.290	0.001	0.694	0.304	0.006
125	0.623	0.374	0.002	0.636	0.357	0.009
150	0.538	0.458	0.004	0.579	0.410	0.011
175	0.492	0.500	0.008	0.543	0.441	0.015
200	0.445	0.543	0.012	0.508	0.473	0.019
250	0.348	0.623	0.029	0.376	0.586	0.038
300	0.250	0.684	0.067	0.315	0.623	0.062
350	0.152	0.744	0.104	0.255	0.660	0.085
400	0.113	0.723	0.164	0.201	0.679	0.120
450	0.074	0.702	0.223	0.148	0.698	0.154
480	···	···	···	0.11	0.68	0.20

[a] Recent experiments by Jorgensen, Kuyatt, and Sauter [Bull. Am. Phys. Soc. Ser. II, 3, 230 (1958)] indicate that $F_{1\infty}$ in H_2 gas reaches a broad maximum between 115 and 155 kev, where it has a value of 2.1×10^{-4}.

some scattered data at higher energies. The data from 4 to 200 kev have been summarized by Barnett and Stier (Ba 58), including graphs of the cross sections *versus* particle velocity. In the present report, the values are tabulated at the various beam energies, with the trends illustrated by graphs showing the effects in hydrogen gas.

(*1*) *Measurements of Equilibrium Fractions*

Experimental values for $F_{0\infty}$, $F_{1\infty}$, and $F_{2\infty}$ for helium beams in gases are given in Tables VI-1 to VI-4. The main sources of direct measurement of these fractions are Snitzer (Sn 53), and Barnett and Stier (Ba 58a).

TABLE VI-2. Equilibrium fractions for a helium beam in the target gases N_2 and O_2 (Ba 58).

Kinetic energy (kev)	Nitrogen gas			Oxygen gas		
	$F_{0\infty}$	$F_{1\infty}$	$F_{2\infty}$	$F_{0\infty}$	$F_{1\infty}$	$F_{2\infty}$
4	0.980	0.020	···			
8	0.963	0.037	···	0.973	0.027	···
12	0.946	0.054	···	0.946	0.054	···
16	0.928	0.072	···	0.929	0.071	···
20	0.906	0.094	···	0.903	0.097	···
40	0.810	0.190	···	0.780	0.220	···
60	0.725	0.275	···	0.705	0.293	0.0021
80	0.650	0.348	0.0023	0.640	0.356	0.0040
100	0.590	0.406	0.0041	0.585	0.408	0.0069
125	0.518	0.474	0.0084	0.524	0.464	0.012
150	0.455	0.530	0.015	0.471	0.511	0.018
175	0.396	0.580	0.024	0.421	0.556	0.029
200	0.340	0.625	0.035	0.378	0.588	0.034

In the pioneer work of Snitzer, thermistor detectors were used and the flux of particles in the various charge states of the equilibrated beam were measured calorimetrically, after magnetic analysis. Snitzer's results were listed in full in Allison and Warshaw (Al 53). Subsequent experimentation has in general verified the correctness of the ratio $F_{2\infty}/F_{1\infty}$ found by Snitzer, but indicates that Snitzer's $F_{0\infty}$ values are from 15 to 20% too low in the region 100 to 200 kev. In the present review the results of Snitzer are listed only if no other data are available for the target gas and helium particle energy. The equilibrium fractions in the target gases H_2, Ne, N_2, O_2, Ne, and A in the kinetic energy range 4 to 200 kev are taken from Table I of reference (Ba 58). It is also possible to compute $F_{i\infty}$ values, using Eqs. (II-16) to (II-18) and a set of cross-section values. This has been done, using values of σ_{if} by Allison *et al.* (Al 56) and by Allison (Al 58) in the energy range 100 to 450 kev, for target gases H_2, He, and air. In the gases H_2 and He, and the kinetic energy range 100 to 200 kev, where they overlap the directly measured results of Barnett and Stier, the agreement is satisfactory. The tabulated $F_{i\infty}$ values for these gases from 200 to 450 kev were computed as indicated, and the values for air in Table VI-3 were obtained in this manner also. Figure VI-1 shows the equilibria in the target gas helium in graphical form.

Unless He^- or He^0 ions are artificially prepared at high energy before equilibration, helium is essentially a two-component system above 1 Mev, and the cross sections σ_{12} and σ_{21} reported by Rutherford (Ru 24) as listed in Table VI-8 can be used to compute $F_{1\infty}$ in air from equations analogous to (II-33) and (II-34). Negative helium ions have been observed by Dukel'skii *et al.* (Du 56) and their values of the cross sections for their formation are discussed in the subsequent

TABLE VI-3. Equilibrium fractions for a helium beam in air (computed from cross-section determinations).

Kinetic energy (kev)	$F_{0\infty}$	$F_{1\infty}$	$F_{2\infty}$
100	0.639	0.358	0.004
125	0.565	0.427	0.008
150	0.483	0.506	0.012
175	0.442	0.540	0.0175
200	0.398	0.578	0.024
250	0.331	0.619	0.050
300	0.293	0.630	0.077
350	0.226	0.647	0.127
400	0.180	0.640	0.180
450	0.118	0.645	0.238
480[a]	0.055	0.66	0.29
646[b]		0.50	0.50
1696[b]		0.12	0.88
4440[b]		0.015	0.985
6780[b]		0.005	0.995

[a] From reference (Sn 53).
[b] From reference (Ru 24).

section. Although they did not measure $F_{\bar{1}\infty}$ directly, it is stated by them that at 80 kev, a beam issuing from a collision chamber 16 cm long containing argon at 2.5×10^{-4} mm $[(pl)=4]$ contained 1.4×10^{-12} amp of He^-. Since the original He^+ current was 3.3×10^{-7} amp, this makes $F_{\bar{1}}/F_1=4\times10^{-6}$. The (pl) value was probably too low for them to complete the equilibration, but $F_{\bar{1}\infty}$ was certainly very small.

Windham *et al.* (Wi 58) have formed He^- by passing an intense 17.5 kev He^+ beam through a collision chamber containing hydrogen. It may be inferred from their paper that $F_{\bar{1}\infty}/F_{1\infty}\sim5\times10^{-6}$ under these conditions. Their work is further discussed in the following section.

Recently Dahl *et al.* (Da 57), using the same arrangement as Windham *et al.*, have obtained negative helium in amounts as large as 5×10^{-8} amp. (See also footnote a to Table VI-1.)

(2) *Measurement of Charge-Changing Collision Cross Sections*

Some experimental results for the cross-sections σ_{if} for charge changing collisions of helium particles are given in Tables VI-5 to VI-11. In several publications during approximately the period 1936–1939, Wolf (Wo 37) reported an extensive series of measurements on charge-changing collisions, some of which were on hydrogen and helium beams in the energy range covered by this review. Wolf's results have been reported graphically by Massey and Burhop (Ma 52), and in the paper by Hasted and Stedeford (Ha 55). Wolf's results are not included in the tables presented here. This

TABLE VI-4. Equilibrium fractions for a helium beam in the target gases neon and argon.

Kinetic energy (kev)	Neon gas			Argon gas		
	$F_{0\infty}$	$F_{1\infty}$	$F_{2\infty}$	$F_{0\infty}$	$F_{1\infty}$	$F_{2\infty}$
8	0.982	0.018	···	0.995	0.005	···
12	0.970	0.030	···	0.984	0.016	···
16	0.959	0.041	···	0.976	0.024	···
20	0.940	0.060	···	0.972	0.028	···
40	0.835	0.164	0.0012	0.885	0.115	···
60	0.745	0.251	0.0014	0.800	0.200	···
80	0.672	0.320	0.0078	0.720	0.279	0.0012
100	0.609	0.379	0.012	0.652	0.345	0.0026
125	0.548	0.435	0.017	0.572	0.428	0.0052
150	0.495	0.482	0.023	0.499	0.500	0.0092
175	0.449	0.521	0.029	0.425	0.560	0.0155
200	0.414	0.551	0.035	0.372	0.604	0.024
250[a]	···	···	···	0.20	0.76	0.047
300[a]	···	···	···	0.15	0.77	0.085
350[a]	···	···	···	0.10	0.74	0.14
400[a]	···	···	···	0.07	0.71	0.22
450[a]	···	···	···	0.05	0.65	0.29
480[a]	···	···	···	0.045	0.62	0.33

[a] From reference (Sn 53).

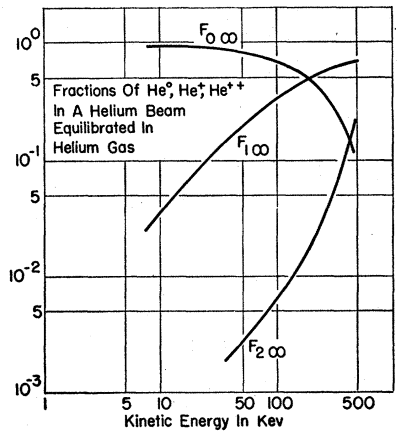

FIG. VI-1. Equilibrium fractions of He^0, He^+, and He^{++} in the target gas helium.

energy region, 0.2 to 2.5 kev, has been explored by Hasted (Ha 51, 52, 55) and, in general, Hasted's results join on smoothly with those of other investigators who have extended his range to higher energies. The same

TABLE VI-5. Charge-changing cross sections for He^0 and He^+ in hydrogen gas. Cross sections in units of 10^{-17} cm² per atom of hydrogen.

Kinetic energy (kev)	σ_{01}	σ_{10}			
	(Ba 58)	(Ha 55)	(St 55)	(He 56)	(Ba 58)
0.2		7.5			
0.4		7.0			
0.6		6.5			
0.8		6.0			
1.0		5.5			
2		4.2			
3		4.0	3.5		
4	0.25		3.5		
5			4.0		
6			4.2		
7			4.6		
8	0.70		4.7		3.9
12	1.0		5.7	6.4	5.4
16	1.5		7.5	7.9	6.8
20	1.8		7.8	10.1	8.0
25			8.5		
30	2.0		10		10.5
35			11		
40	2.4		12		11
60	3.0				
80	3.9				12

	σ_{01}	σ_{02}	σ_{10}	σ_{12}	σ_{20}	σ_{21}
100	4.2		9.8	0.13		38
125	5.1		8.7	0.18		32
150	5.5		7.1	0.24	1.1	26
175	5.8		5.7	0.37	1.0	24
200	5.9		4.8	0.50	0.98	21
250	6.0		3.2	0.64	0.87	14
300	6.2		2.2	0.81	0.53	11
350	6.2	<0.1	1.2	0.98	0.20	6.8
400	6.3		0.95	0.89	0.16	4.9
450	6.7	<0.1	0.70	0.80	0.12	2.4

TABLE VI-6. Charge-changing cross sections for He^0, He^+, and He^{++} in helium gas. Cross sections in units of 10^{-17} cm² per atom of target helium.

Kinetic energy (kev)	σ_{01} (Ru 31)	σ_{01} (Ba 58)	σ_{11} (Du 56)	σ_{10} (Ru 31)	σ_{10} (Ha 55)	σ_{10} (St 55)	σ_{10} (Ba 58)
0.2					108		
0.4					95		
0.6					92		
0.8					86		
1.0					82		
2					70	82	
3						78	72
4		0.46				74	
5	0.93					72	
6						69	
7						66	
8	1.8	1.8		34		63	60
12	2.9	3.0		33		58	58
16	3.8	4.0		31		55	53
20	4.1	4.8		29		52	50
25						48	
30		5.9				44	43
35						39	
40		6.2				38	38
60		7.3	0.0_32				30
80		8.0	0.0_32				24

	σ_{01}	σ_{02}	$\sigma_{1\bar{1}}$	σ_{10}	σ_{12}	σ_{20}	σ_{21}
100	7.6		0.0_32	17	0.56	$\sigma_{20}+\sigma_{21}=38$	
125	8.5		0.0_32	15	0.60	$\sigma_{20}+\sigma_{21}=26$	
150	9.0		0.0_32	12	0.64	5.7	19
175	9.4		0.0_32	10	0.76	4.7	17
200	9.7		...	8.6	0.88	3.7	15
250	9.9		...	6.2	1.0	2.7	14
300	9.8		...	4.4	1.2	1.9	12
350	9.4	<0.2	...	3.1	1.5	1.1	11
400	8.9	...	...	2.2	1.9	1.1	9.2
450	8.2	<0.2	...	1.5	2.1	1.1	7.5

comment applies to the work of Rostagni (Ro 36, 38) who studied the charge-changing behavior of charged ions of helium, neon, and argon in these cases, respectively. The results of Smith (Sm 34) on σ_{10} for He^+ in helium cover the energy range 2 to 12 kev, but with the exception of his values at 2 and 4 kev they are not in agreement with those tabulated.

The results of Keene (Ke 49) on charge-changing collisions of H^+ and He^+ ions are also not tabulated. Keene's measurements were repeated, with minor modifications of the apparatus, by Stedeford (St 55) and cross sections considerably smaller than Keene's were found. Apparently some systematic error was present in Keene's measurements.

TABLE VI-7. Charge-changing cross sections for He^0, He^+ in nitrogen and oxygen gases. Cross sections in units of 10^{-17} cm² per atom of target gas.

Kinetic energy (kev)	Nitrogen σ_{01}	Nitrogen σ_{10}	Oxygen σ_{01}	Oxygen σ_{10}
4	...	...	0.27	...
8	0.83	21.5	1.1	39
12	1.7	27	2.2	39
16	2.3	30	3.2	41
20	3.2	32	4.5	41
40	7.2	32	9.3	34
60	11	29	14	30
80	14	26	16	28
100	16	24	17.5	24
125	19	20	19.5	20
150	20	18	20	19
175	23	15	22	16
200	24	13	23	15

TABLE VI-8. Charge-changing cross sections for helium beams in air (in units of 10^{-17} cm² per atom).

Kinetic energy (kev)	σ_{01}	σ_{02}	σ_{10}	σ_{12}	σ_{20}	σ_{21}
100	16.4	...	29	0.79	$\sigma_{20}+\sigma_{21}=79$	
150	21.0	0.2±0.2	20	1.2	11.8	50
200	21.8	...	16	2.2	8.5	42
250	22.7	0.5±0.4	12	3.1	5.2	35
350	21.2	0.8±0.5	7.3	5.1	2.1	25
450	23.2	1.3±0.4	4.0	6.6	1.3	17
646	...	...	...	6.2	...	6.2
1696	...	...	...	3.7	...	0.50
4440	...	...	...	2.4	...	0.036
6780	...	...	...	1.68	...	0.0084

TABLE VI-9. Charge-changing cross sections for He^0 and He^+ in neon gas. Cross sections in units of 10^{-17} cm² per neon atom.

Kinetic energy (kev)	σ_{01} (Ba 58)	$\sigma_{1\bar{1}}$ (Du 56)	σ_{10} (Ha 55)	σ_{10} (St 55)	σ_{10} (Ba 58)
0.2			2		
0.4			3		
0.6			5		
0.8			8		
1.0			11		
2			23		
3			38	42	
4	0.42			58	
5				65	
6				74	
7				75	
8	1.4			75	71
12	2.2			73	71
16	3.1				69
20	4.2				65
30	7.5	0.0_35		60	50
40	8.6	0.0_38		53	43
50	11.5	0.0_39			33
60	12	0.0011			35
70	14.5	0.0012			29
80	15	0.0011			30
100	16	0.0010			24
125	17.5	0.0_38			20.5
150	18.5	0.0_35			19
175	19.5	0.0_33			16.5
200	20				15.5

Measurements on helium ions were made by Meyer (Me 37, 40) but are not tabulated here. They are shown graphically in the joint paper by Hasted and Stedeford (Ha 55, St 55). The measurements by Hasted (Ha 51, 52) prior to his joint publication with Stedeford in 1955 are not separately tabulated.

In Tables VI-5, VI-6, and VI-8 the cross sections from 100 to 450 kev are essentially those of Allison *et al.* (Al 56) and Allison (Al 58, 58a) although in computing σ_{10} and σ_{12} use has been made of equilibrium fractions observed by Snitzer (Sn 53) and by Barnett and Stier (Ba 58).

Values of $(\sigma_{01}+\sigma_{02})$ for He^0 measured by Krasner (Kr 55) are not included in the present tables. Krasner's measurements, with some improvements in his apparatus, have been repeated (Al 58a) and it is apparent that his cross sections were too large due to some unknown systematic error.

The values of σ_{01} and σ_{10} for He^0 and He^+ in nitrogen and oxygen (Table VI-7) are due to Barnett and Stier (Ba 58).

In Table VI-8 the cross sections in air above 450 kev kinetic energy are due to Rutherford (Ru 24) who used RaC′ α particles.

The sources for the data on the charge-changing collisions of He^0 and He^+ in the noble gases are given in the column headings (Tables VI-9 to VI-11).

TABLE VI-10. Charge-changing cross sections for He^0 and He^+ in argon gas. Cross sections in units of 10^{-17} cm² per argon atom.[a]

Kinetic energy (kev)	σ_{01} (Ba 58)	$\sigma_{1\bar{1}}$ (Du 56)	σ_{10} (Ha 55)	σ_{10} (St 55)	σ_{10} (Ba 58)
0.2			10		
0.4			13		
0.6			15		
0.8			19		
1.0			21		
2			30		
3			34	35	
4				42	
5				49	
6				50	
7				52	
8	0.42			55	51
12	0.95			65	58
16	1.6			66	63
20	2.3	0.001		67	75
30	4.5	0.003		68	66
40	8.0	0.0055		68	61
50	12	0.0065			63
60	16	0.0075			60
70	18	0.007			57
80	20	0.006			52
100	24				46
125	28				36
150	31				31
175	36				26
200	39				23

[a] At 10 kev, de Heer (He 56) obtained $\sigma_{01}=5.8$; $\sigma_{10}=70$ or 53 using different methods.

TABLE VI-11. Charge-changing cross sections for He^0 and He^+ in krypton and xenon gas. Cross sections in units of 10^{-17} cm² per target atom.

Kinetic energy (kev)	Krypton $\sigma_{1\bar{1}}$ (Du 56)	Krypton σ_{10} (Ha 55)	Krypton σ_{10} (St 55)	Xenon σ_{10} (Ha 55)	Xenon σ_{10} (St 55)
0.2		10		136	
0.4		20		132	
0.6		29		130	
0.8		40		125	
1.0		50		123	
2		71		110	176
3		73	82	106	140
4			85		128
5			86		120
6			86		118
7			87		114
8			87		110
12			88		105
16			89		100
20	0.0035		90		98
30	0.008		90		110
40	0.012		90		109
50	0.014				
60	0.015				
70	0.014				
80	0.013				
100	0.010				
125	0.0077				
150	0.0070				
175	0.005				

A serious discrepancy exists in the measurements in xenon. The low-energy data of Hasted do not join with the values by Stedeford where the regions of measurement overlap between 2 and 3 kev kinetic energy.

Negative helium.—Although from general considerations it would be predicted that He^- would be one of the least stable electronegative ions, recent theoretical work by Holøien and Mitdal (Ho 55) has indicated the possibility that such a combination having an electron affinity of 0.075 ev could exist for as long as 10^{-3} sec under experimental conditions in high vacuum [see also the work by Ta-You Wu (Ta 36)]. Hiby (Hi 39) reported He^- as observed in a J. J. Thomson parabolic analysis of canal rays from a helium discharge. The production of He^- by means of charge-changing collisions beginning with He^+ has been reported by Dukel'skii *et al.* (Du 56), in which minute amounts of He^- were observed to emerge from a collision chamber in which a He^+ beam was allowed to interact with the noble gases. The growth of He^- from He^+ was linear up to pressures of 5×10^{-4} mm in a collision chamber 16 cm long, indicating that it was produced through double electron capture in a single collision of He^+ with a noble gas atom. The cross sections observed by Dukel'skii *et al.* are listed in the tables in this section.

Windham *et al.* (Wi 58) have also observed He^- produced by allowing an intense He^+ beam of 17.5 kev

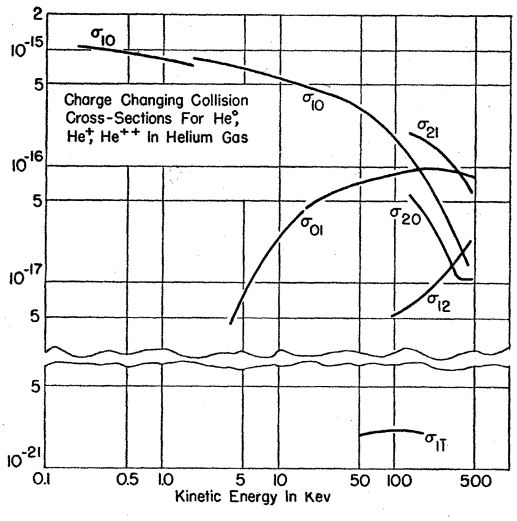

FIG. VI-2. The charge-changing cross sections for He^0, He^+, and He^{++} in the target gas helium. Ordinates are in cm^2.

kinetic energy to pass through a collision chamber containing hydrogen gas. They observed a maximum in the ratio $F_{\bar{1}}/F_1$ at approximately $(pl)=25\,\mu\times$cm, and using considerations similar to those of Sec. III-A, they make the rough estimates that $\sigma_{1\bar{1}}=10^{-20}$ cm^2 and $(\sigma_{\bar{1}0}+\sigma_{\bar{1}1})\sim(2.1\pm1.5)\times10^{-15}$ cm^2. These values are not included in the tables.

The cross sections in helium gas are displayed graphically in Fig. VI-2. The same general features are to be seen in all target gases; the energy at which $\sigma_{01}=\sigma_{10}$ appears to be somewhat smaller in heavier gases than in H_2 and He.

(3) *Stages in the Charge Equilibration of Helium Beams*

The growth of new charge fractions F_i in a helium beam passing from medium 1 into medium 2 in which the equilibrium fractions F_i have new values, can be computed from Eq. (II-12). The quantities q, $F_{i\infty}$, and $\frac{1}{2}\sum\sigma_{if}$ which appear are independent of the charge composition of the beam in medium 1. The values of $F_{i\infty}$ have been given in Tables VI-1 to VI-4. Table VI-12 gives values of q and $\frac{1}{2}\sum\sigma_{if}$ in the energy range 100 to 450 kev. Except in quite unusual situations, two components suffice to describe the helium system at energies below and above this region, where the system contains only He^0 and He^+, or He^+ and He^{++} respectively.

TABLE VI-12. Quantities useful in the calculation of the change of charge of a helium beam using Eq. (II-12).

Kinetic energy (kev)	Hydrogen $\frac{1}{2}\Sigma\sigma_{if}\times10^{17}$	Hydrogen $10^{17}q$	Helium $\frac{1}{2}\Sigma\sigma_{if}\times10^{17}$	Helium $10^{17}q$	Air $\frac{1}{2}\Sigma\sigma_{if}\times10^{17}$	Air $10^{17}q$
100	26.0	12.9	26.5	3.19	62.6	17.6
125	23.0	...	25.0			
150	20.2	7.66	23.3	2.89	52.1	11.3
175	16.6	...	20.9			
200	16.6	...	19.0		45.2	
250	12.1	3.20	16.9	1.80	39.2	5.83
300	10.4	...	14.6			
350	7.6	1.06	12.4	1.93	30.8	4.95
400	6.6	...	11.8			
450	5.5	2.29	10.1	0.96	26.7	4.19

The only charge-changing cases which have been calculated are those in which medium 1 is a vacuum, in which there is a selected beam, all of whose particles are in the same initial charge state $z|e|$ where $|e|$ is the magnitude of the electronic charge. Tables VI-13 and VI-14 show the values of $P(z,i)$ and $N(z,i)$ for such helium beams of unmixed charge state entering the target gases hydrogen, helium, or air. As an example of the use of these tables, the fraction of He^+ at 450 kev, converted to He^{++} in a collision chamber 10 cm long at 3 μ air pressure is computed as follows. From Eq. (II-12)

$$F_2=F_{2\infty}+[P(1,2)\exp(\pi q)+N(1,2)\exp(-\pi q)]\exp(-\tfrac{1}{2}\pi\textstyle\sum\sigma_{if}),$$

$F_{2\infty}=0.238$ (Table VI-3),

$P(1,2)$; $N(1,2)$ are -0.095 and -0.143, respectively (Tables VI-13, VI-14),

$\pi=30\times6.61\times10^{13}=1.98\times10^{15}$ atoms/cm^3 [from Eqs. (V-1) and (V-2)],

$\frac{1}{2}\sum\sigma_{if}$ and q are 2.67×10^{-16} and 4.19×10^{-17} cm^2, respectively (Table VI-12).

The result, $F_2=0.10$, is plotted in Fig. VI-4.

The results of the computation of some cases of charge conversion are shown in Figs. VI-3 to VI-7. In Fig. VI-3, the process of conversion of a 450-kev helium atomic beam into the charge types He^+ and

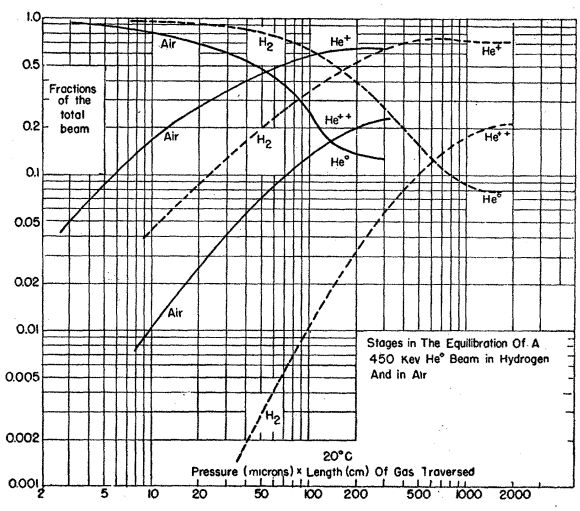

FIG. VI-3. Growth of He^+ and He^{++}, and decay of He^0 in an originally pure, 450 kev atomic helium beam traversing hydrogen or air.

TABLE VI-13. Coefficients $P(z,i)$ for computing helium beam compositions from Eq. (II-12).

kev	$P(0,0)$	$P(0,1)$	$P(0,2)$	$P(1,0)$	$P(1,1)$	$P(1,2)$	$P(2,0)$	$P(2,1)$	$P(2,2)$
					Hydrogen				
100	0.291	−0.289	−0.001	−0.708	0.705	0.002	−1.019	1.015	0.004
150	0.461	−0.454	−0.007	−0.533	0.525	0.009	−0.905	0.891	0.014
250	0.644	−0.594	−0.050	−0.327	0.300	0.027	−0.697	0.641	0.056
350	0.626	−0.204	−0.422	−0.059	0.019	0.040	−0.531	0.173	0.358
450	0.049	+0.331	−0.379	+0.027	0.179	−0.205	−0.100	−0.672	0.772
					Helium				
100	0.266	−0.236	−0.030	−0.574	0.507	0.067	−2.092	1.846	0.243
150	0.370	−0.322	−0.048	−0.483	0.416	0.067	−1.635	1.425	0.210
250	0.484	−0.341	−0.143	−0.231	0.163	0.068	−1.212	0.854	0.358
350	0.580	−0.267	−0.312	−0.140	0.064	0.075	−0.658	0.303	0.355
450	0.636	+0.253	−0.889	−0.073	−0.029	−0.102	−0.281	−0.112	0.393
					Air				
100	0.360	−0.349	−0.011	−0.632	0.614	0.018	−0.939	0.912	0.027
150	0.511	−0.488	−0.023	−0.472	0.150	0.021	−0.835	0.798	0.038
250	0.598	−0.441	−0.157	−0.250	0.185	0.066	−0.833	0.614	0.219
350	0.566	−0.185	−0.380	−0.080	0.026	0.054	−0.606	0.198	0.407
450	0.329	+0.401	−0.730	+0.043	0.052	−0.095	−0.279	−0.340	0.619

He^{++} in the target gases hydrogen or air is shown. In hydrogen 92.5% of the atomic beam can ultimately be changed into He^{+} and He^{++}; in air 88.3% can be so transformed. At 20°C, the conversion in hydrogen is within a few percent of completion at $(pl)=1500\ \mu$ cm; in air only 250 μ cm are required.

Figure VI-4 gives the charge conversion of a 450-kev He^{+} beam in hydrogen and air, and Fig. VI-5 gives similar information for a 450-kev He^{++} beam. Figures VI-6 and VI-7 are of interest in the preparation of He^{++} beams for acceleration. They show the (pl) values necessary to produce He^{++} from a He^{+} beam, at various kinetic energies, in the target gases H_2 and air. An ion source which produces He^{++} from He^{+} has been described by Bittner (Bi 54).

B. Helium Beams Equilibrated in Solids

The discovery by Henderson in 1922 (He 22) that α particles emitted from a radioactive source always show evidence of a singly charged component initiated several experimental measurements on $F_{2\infty}/F_{1\infty}$ for helium beams equilibrated in solids (Ru 24, Br 27, He 25, Ja 27). Measurements were made on the α

TABLE VI-14. Coefficients $N(z,i)$ for computing helium beam compositions from Eq. (II-12).

kev	$N(0,0)$	$N(0,1)$	$N(0,2)$	$N(1,0)$	$N(1,1)$	$N(1,2)$	$N(2,0)$	$N(2,1)$	$N(2,2)$
					Hydrogen				
100	0.001	−0.001	−0.001	−0.001	0.005	−0.004	0.310	−1.304	0.995
150	0.001	−0.004	0.003	−0.004	0.017	−0.013	0.367	−0.349	0.982
250	0.008	−0.029	0.027	−0.021	0.077	−0.056	0.349	−1.264	0.915
350	0.222	−0.540	0.318	−0.093	0.237	−0.144	0.379	−0.917	0.539
450	0.975	−1.033	0.756	−0.101	0.119	−0.018	0.026	−0.030	0.004
					Helium				
100	0.044	−0.068	0.024	−0.120	0.189	−0.073	1.383	−1.556	0.751
150	0.052	−0.088	0.036	−0.096	0.174	−0.078	1.256	−1.837	0.581
250	0.140	−0.245	0.105	−0.145	0.251	−0.136	1.056	−1.440	0.604
350	0.166	−0.393	0.232	−0.115	0.276	−0.160	0.403	−0.963	0.560
450	0.216	−0.951	0.736	−0.075	0.331	−0.256	0.133	−0.586	0.453
					Air				
100	0.002	−0.009	−0.007	−0.067	0.028	−0.022	0.300	−1.269	0.969
150	0.006	−0.018	0.012	−0.011	0.044	−0.033	0.352	−1.304	0.951
250	0.071	−0.178	0.106	−0.080	0.196	−0.116	0.502	−1.233	0.731
350	0.208	−0.462	0.254	−0.146	0.327	−0.181	0.380	−0.846	0.466
450	0.553	−1.046	0.493	−0.161	0.303	−0.143	0.161	−0.305	0.144

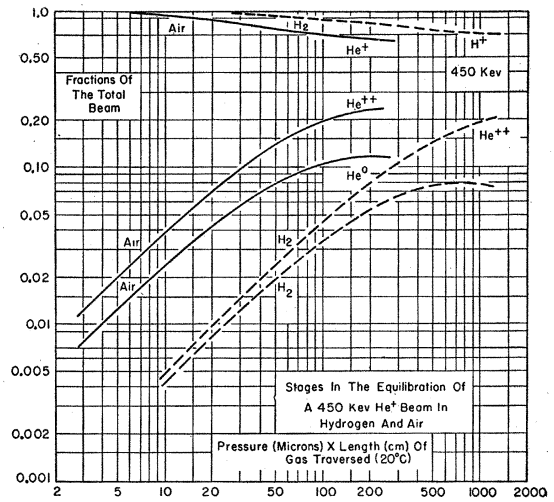

FIG. VI-4. Growth of He^0 and He^{++}, and decay of He^+ in an originally pure, 450 kev He^+ beam traversing hydrogen or air.

particles from RaC′ ($_{84}Po^{214}$) as they left the solid source with 7680 kev kinetic energy and after slowing them down by interposition of mica foils. The data given on $F_{1\infty}$ after passage through foils of mica, Al, Cu, Ag, and Au in Table VI-15 are from the work of Rutherford (Ru 24) and of Henderson (He 25). The α's were magnetically analyzed and counted by the scintillation method. At all the listed energies higher than 406 kev, the fraction $F_{0\infty}$ is negligible, and $F_{1\infty}$ may be inferred from the reported measurements, which are of $F_{1\infty}/F_{2\infty}$. The tabulated value of 0.68 for $F_{1\infty}$ at 406 kev has been computed from Rutherford's original observations on the assumption that $F_{0\infty}$ was **0.1.**

Dissanaike (Di 53) has made a survey of the fractions of He^0, He^+, and He^{++} present in helium ions scattered

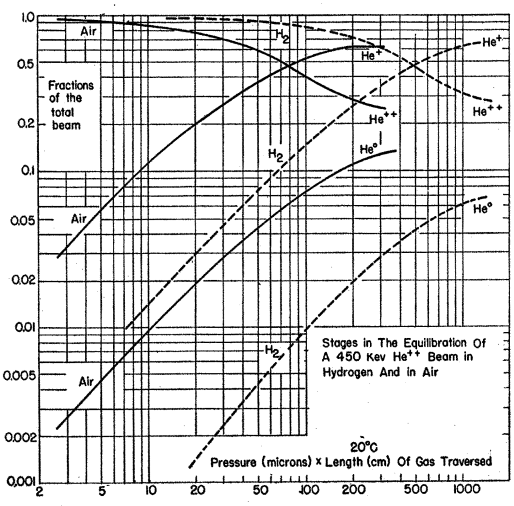

FIG. VI-5. Growth of He^0 and He^+, and decay of He^{++} in an originally pure, 450 kev He^{++} beam traversing hydrogen or air.

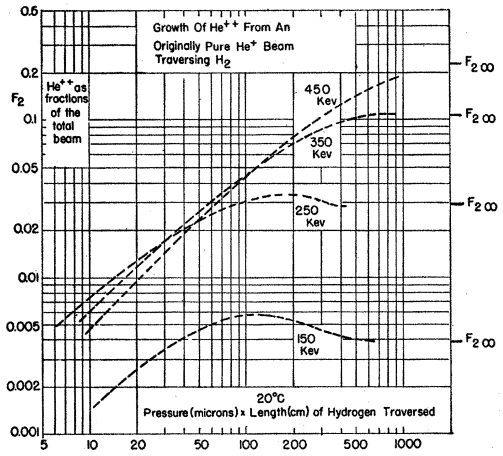

FIG. VI-6. Growth of He^{++} in an originally pure He^+ beam traversing hydrogen gas. Kinetic energies from 150 to 450 kev.

at 90° from thin foils of Be, Al, Hg, in the kinetic energy range 130 to 1100 kev. The plane of the scattering foils was inclined at 45° to the incident helium ion beam, and the charge analysis was made on those particles which had been scattered 90°, and had emerged from the far side of the foil. In the case of the charged particles, where the energy could be determined by magnetic deviation, scattering foils having from 0.03 and 0.07 cm air equivalent at NTP were used [(pl) values from 23×10^3 to 53×10^3]. Thus, by comparison with Figs. VI-3, VI-4, and VI-5, the foils were on the order of 100 to 300 times as thick as necessary to produce charge equilibrium. For the analysis of the neutral fraction, where the emergent energy could not be magnetically determined and it was desirable to minimize energy straggling in the foil, foils of Ag and Al of stopping power between 0.015 and 0.03 cm of air were used. Zinc sulfide scintillations, counted by a photomultiplier tube circuit were used

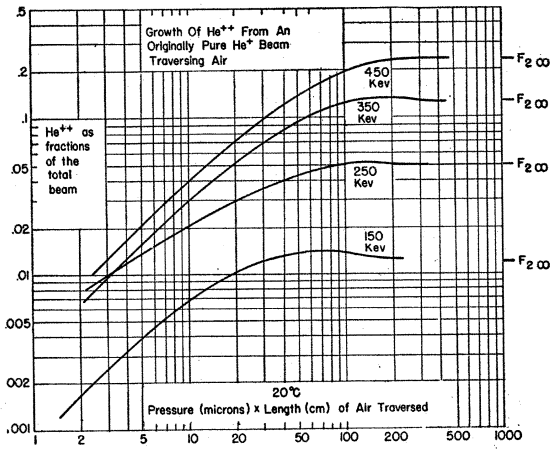

FIG. VI-7. Growth of He^{++} in an originally pure He^+ beam traversing air. Kinetic energies from 150 to 450 kev.

for the charged particle components, and also an electron multiplier tube of the Allen type (Ro 48) was used. Dissanaike's results are listed in the first three data columns of Table VI-15.

At the time of preparation of the Allison and Warshaw review (Al 53) the results of Dissanaike were not available and some provisional and unpublished results of Allison, Casson, and Weyl were presented, showing $F_{2\infty}/F_{1\infty}$ determinations on helium ions scattered from gold and nickel. These results are not in satisfactory agreement with those of Dissanaike; particularly at energies between 200 and 300 kev where the $F_{2\infty}/F_{1\infty}$ ratios run 60% higher than his. The results of Allison *et al.* are not included in the present review.

There is considerable interest in the question as to whether the same charge equilibria are produced in substances as physically different as gases and solid metals. Evidence that the equilibrium fractions from solids are shifted toward larger amounts of electron deficient ions was presented in the review of Allison and Warshaw (Al 53, Fig. 17). The more recent data still indicate that this may be the case, between 100 and 400 kev kinetic energy, for helium particles, but the difference is now not so pronounced. Figure VI-8 shows values of $F_{2\infty}$ obtained by Dissanaike for solid metal foils, compared to data computed from cross sections in air and hydrogen gas obtained by Allison *et al.* (Al 56). In the lower energy range the metallic $F_{2\infty}$ values seem distinctly higher than in the comparison gases, but from Tables VI-4 and VI-15 the $F_{2\infty}$ values on the target gas neon are quite close to those for metals, showing that the physical state of the target material is not the only relevant factor.

In addition, Fig. VI-8 includes the values of $F_{1\infty}$ for hydrogen beams equilibrated in the gases H_2 and N_2 and these are compared with the equilibrium values found by Phillips (Ph 55) from fresh aluminum foils. It is seen that in the metal-equilibrated beam the percent of protons, at the same kinetic energy, is intermediate between that characteristic of H_2 and N_2.

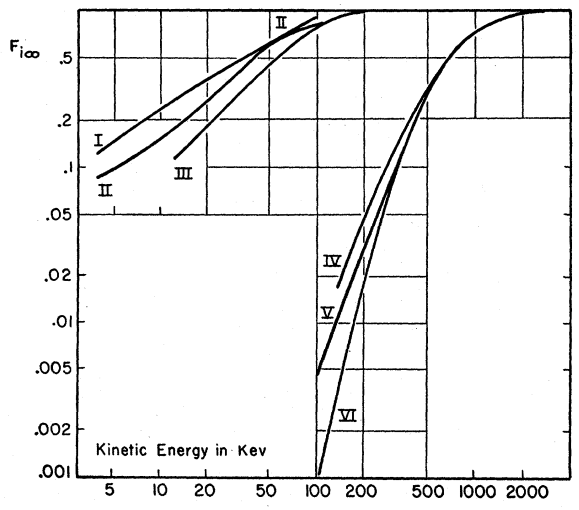

FIG. VI-8. I. $F_{1\infty}$ for hydrogen beams in N_2 gas. II. $F_{1\infty}$ for hydrogen beams emergent from a fresh aluminum surface. III. $F_{1\infty}$ for hydrogen beams in H_2 gas. IV. $F_{2\infty}$ for helium beams scattered from metals. V. $F_{2\infty}$ for helium beams in air. VI. $F_{2\infty}$ for helium beams in H_2 gas.

TABLE VI-15. Charge composition of helium beams equilibrated in solids.

Kinetic energy (kev)	Scattered and transmitted in Be, Al, Ag foils			$F_{1\infty}$ emergent from	
	$F_{0\infty}$	$F_{1\infty}$	$F_{2\infty}$	Mica foil	Au foil
130	0.58	0.40	0.017		
200	0.39	0.57	0.04		
300	0.24	0.65	0.11		
400	0.15	0.65	0.20		
406				0.68	
500	0.09	0.59	0.32		
590				0.60	
600	0.06	0.52	0.42		
640				0.50	
700	0.02	0.43	0.55		
787				0.35	
800		0.36	0.64		
900		0.29	0.71		
1000		0.24	0.76		
1100		0.20	0.80		
1260				0.16	
1355				0.14	0.14
1521				Ag foil 0.12	
1696				0.12	
1935				0.061	0.065
2323				Al foil 0.045	
2408				0.038	0.038
2719				0.032	0.036
3406					0.024
4262				Cu foil 0.015	
4440				0.015	
4915				0.012	
6028				0.0079	0.0088

7684 $F_{1\infty}$ direct from RaC′ source 0.062 (He 25); 0.050 (Ru 24).

REFERENCES

Al 53 S. K. Allison and S. D. Warshaw, Revs. Modern Phys. **25**, 779 (1953).

Al 56 Allison, Cuevas, and Murphy, Phys. Rev. **102**, 1041 (1956).

Al 58 S. K. Allison, Phys. Rev. **109**, 76 (1958).

Al 58a S. K. Allison, Phys. Rev. **110**, 670 (1958).

Ba 55 C. F. Barnett and P. M. Stier, Phys. Rev. **100**, 1268 (1955).

Ba 55a C. F. Barnett and P. M. Stier, Phys. Rev. **30**, 7, 41 (1955).

Ba 58 C. F. Barnett and H. K. Reynolds, Phys. Rev. **109**, 355 (1958).

Ba 58a C. F. Barnett and P. M. Stier, Phys. Rev. **109**, 385 (1958).

Ba 30 H. Bartels, Ann. Physik **6**, 957 (1930).

Ba 32 H. Bartels, Ann. Physik **13**, 373 (1932).

Bi 54 J. W. Bittner, Rev. Sci. Instr. **25**, 1058 (1954).

Bo 48 N. Bohr, Kgl. Danske Videnskab. Selskab. Mat.-fys. Medd. **18**, No. 8 (1948).

Br 27 G. H. Briggs, Proc. Roy. Soc. (London) **A114**, 341 (1927).

Br 30 H. C. Brinkman and H. A. Kramers, Proc. Acad. Sci. Amsterdam **33**, 973 (1930).

Ca 56 Carbone, Fuls, and Everhart, Phys. Rev. **102**, 1524 (1956).
Da 57 Dahl, Brostrom, Greene, Herb, and Peterson, Bull. Am. Phys. Soc. Ser. II, **2**, 338 (1957).
Di 53 G. A. Dissanaike, Phil. Mag. **7**, 44, 1051 (1953).
Du 55 V. N. Dukel'skii and N. V. Fedorenko, Zhur. Eksptl. i Teort. Fiz. **29**, 473 (1955); English transl. Soviet Phys. JETP **2**, 307 (1956).
Du 56 Dukel'skii, Afrosimov, and Fedorenko, Zhur. Eksptl. i Teort. Fiz. **30**, 792; English transl. Soviet Phys. JETP **3**, 764 (1956).
Ev 53 Evans, Stier, and Barnett, Phys. Rev. **90**, 825 (1953).
Fe 54 N. V. Fedorenko, Zhur. Tekh. Fiz. **24**, 769 (1954).
Fe 58 N. V. Fedorenko, Proceedings of the New York University Conference on the Physics of Electronic and Atomic Collisions (January, 1958).
Fo 24 R. H. Fowler, Phil. Mag. **47**, 416.
Fo 55 Fogel, Krupnik, and Safronov, Zhur. Eksptl. i Teort. Fiz. USSR **28**, 589 (1955); English transl. JETP **1**, 415.
Fo 56 Ya. M. Fogel and R. V. Mitin, Zhur. Eksptl. i Teort. Fiz. **30**, 450 (1956); English transl. Soviet Phys. JETP **3**, 334.
Fo 56a Fogel, Safronov, and Krupnik, Zhur. Eksptl. i Teort. Fiz. **28**, 711 (1955); English transl. Soviet Phys. JETP **1**, 546 (1955).
Fo 57 Fogel, Ankudinov, and Slabospitskii, Zhur. Eksptl. i Teort. Fiz. **32**, 453 (1957); English transl. Soviet Phys. JETP **5**, 382.
Fu 57 Fuls, Jones, Ziemba, and Everhart, Phys. Rev. **107**, 704 (1957).
Ge 33 H. Geiger, *Handbuch der Physik* (Verlag Julius Springer, Berlin, 1933), Vol. 22, p. 221.
Ge 54 R. Geller and F. Prevot, Compt. rend. **238**, 1578 (1954).
Ge 55 R. Geller, C.E.A. (France) Report 368.
Go 31 F. Goldmann, Ann. Physik **10**, 460 (1931).
Ha 50 T. Hall, Phys. Rev. **79**, 504 (1950).
Ha 51 J. B. Hasted, Proc. Roy. Soc. (London) **A205**, 421 (1951).
Ha 52 J. B. Hasted, Proc. Roy. Soc. (London) **A212**, 235 (1952).
Ha 53 J. B. Hasted, Proc. Roy. Soc. (London) **A222**, 74 (1953).
Ha 55 J. B. Hasted, Proc. Roy. Soc. (London) **A227**, 466 (1955).
He 22 G. H. Henderson, Proc. Roy. Soc. (London) **A102**, 496 (1922).
He 25 G. H. Henderson, Proc. Roy. Soc. (London) **A109**, 157 (1925).
He 56 F. S. de Heer, Ph.D. thesis, University of Leiden (1956).
Hi 39 J. W. Hiby, Ann. Physik **34**, 473 (1939).
Ho 55 E. Holøien and J. Midtal, Proc. Phys. Soc. (London) **A68**, 815 (1955).
Ja 27 J. C. Jacobsen, Nature **117**, 858 (1927).
Ka 24 P. Kapitza, Proc. Roy. Soc. (London) **106**, 602 (1924).
Ka 30 H. Kallman and B. Rosen, Z. Physik **64**, 806 (1930).
Ka 51 H. Kanner, Phys. Rev. **84**, 1211 (1951).
Ka 55 D. M. Kaminker and N. V. Fedorenko, Zhur. Tekh. Fiz. **25**, 1843 (1955).
Ka 57 W. H. Kasner and T. M. Donahue, Report No. 3 from University of Pittsburgh, Office of Naval Research Project (November, 1957).
Ke 49 J. P. Keene, Phil. Mag. **40**, 7, 369 (1949).
Kr 55 S. Krasner, Phys. Rev. **99**, 520 (1955).
La 55 N. O. Lassen, Kgl. Danske Videnskab. Selskab. Mat.-fys. Medd. **30**, No. 8 (1955).
Ma 52 H. S. W. Massey and E. H. S. Burhop, *Electronic and Ionic Impact Phenomena* (Clarendon Press, Oxford, England, 1952).
Me 37 H. Meyer, Ann. Physik **30**, 635 (1937).
Me 40 H. Meyer, Ann. Physik **37**, 69 (1940).
Mo 51 J. H. Montague, Phys. Rev. **81**, 1026 (1951).
Op 28 J. R. Oppenheimer, Phys. Rev. **31**, 349 (1928).
Ph 53 J. A. Phillips, Phys. Rev. **91**, 455(A) (1953).
Ph 55 J. A. Phillips, Phys. Rev. **97**, 404 (1955).
Ph 56 J. A. Phillips and J. C. Tuck, Rev. Sci. Instr. **27**, 97 (1956).
Ri 51 F. Ribe, Phys. Rev. **83**, 1217 (1951).
Ro 34 A. Rostagni, Z. Phys. **88**, 55 (1934).
Ro 35 A. Rostagni, Nuovo cimento **12**, 134 (1935).
Ro 36 A. Rostagni, Nuovo cimento **13**, 389 (1936).
Ro 38 A. Rostagni, Nuovo cimento **15**, 117 (1938).
Ro 48 L. del Rosario, Phys. Rev. **74**, 304 (1948).
Ro 58 Rose, Connor, and Bastide, Bull. Am. Phys. Soc. Ser. II, **3**, 40 (1958).
Rü 20 A. Rüttenauer, Z. Physik **1**, 385 (1920).
Rü 33 E. Rüchardt, *Handbuch der Physik* (Verlag Julius Springer, Berlin, 1933), Vol. 22, p. 103.
Ru 24 E. Rutherford, Phil. Mag. **47**, 277 (1924).
Ru 31 P. Rudnick, Phys. Rev. **38**, 1342 (1931).
Ru 31a Rutherford, Chadwick, and Ellis, *Radiations from Radioactive Substances* (Cambridge University Press, New York, 1931).
Sc 54 H. Schiff, Can. J. Phys. **32**, 393 (1954).
Sm 34 R. A. Smith, Proc. Cambridge Phil. Soc. **30**, 514 (1934).
Sn 53 E. Snitzer, Phys. Rev. **89**, 1237 (1953).
St 54 Stier, Barnett, and Evans, Phys. Rev. **96**, 973 (1954).
St 55 J. B. A. Stedeford, Proc. Roy. Soc. (London) **A227**, 466 (1955).
St 56 P. M. Stier and C. F. Barnett, Phys. Rev. **103**, 896 (1956).
Ta 36 Ta-You Wu, Phil. Mag. **22**, 837 (1936).
Th 27 L. H. Thomas, Proc. Roy. Soc. (London) **114**, 561 (1927).
Wh 57 Ward Whaling (to be published).
Wh 54 A. C. Whittier, Can. J. Phys. **32**, 275 (1954).
Wi 08 W. Wien, Ann. Physik **27**, 1025 (1908).
Wi 11 W. Wien, Berlin. Ber. 773 (1911).
Wi 12 W. Wien, Ann. Physik **39**, 528 (1912).
Wi 58 Windham, Joseph, and Weinman, Phys. Rev. **109**, 1193 (1958).
Wo 32 F. Wolf, Z. Physik **74**, 575 (1932).
Wo 35 F. Wolf, Ann. Physik **23**, 285, 627 (1935).
Wo 36 F. Wolf, Ann. Physik **25**, 527, 737 (1936).
Wo 36a F. Wolf, Ann. Physik **27**, 543 (1936).
Wo 37 F. Wolf, Ann. Physik **29**, 33 (1937).
Wo 37a F. Wolf, Ann. Physik **30**, 313 (1937).

A BIBLIOGRAPHY OF THEORETICAL PAPERS RELATING TO CHARGE-CHANGING COLLISIONS

Ba 52 D. R. Bates and A. Delgarno, Proc. Phys. Soc. (London) **65**, 919 (1952).
Ba 53 D. R. Bates and G. Griffing, Proc. Phys. Soc. (London) **66**, 961 (1953).
Ba 53a D. R. Bates and G. Griffing, Proc. Phys. Soc. (London) **66**, 972 (1953).
Ba 54 D. R. Bates and G. W. Griffing, Proc. Phys. Soc. (London) **67**, 663 (1954).
Ba 54a D. R. Bates and B. L. Moisiewitsch, Proc. Phys. Soc. (London) **67**, 805 (1954).
Ba 55 D. R. Bates and G. W. Griffing, Proc. Phys. Soc. (London) **68**, 90 (1955).
Be 53 G. I. Bell, Phys. Rev. **90**, 548 (1953).
Bo 40 N. Bohr, Phys. Rev. **58**, 654 (1940).
Bo 54 N. Bohr and A. Lindhard, Kgl. Dan. Videnskab. Selskab. Mat.-fys. Medd. **28**, 7 (1954).
Bo 57 Boyd, Moiseiwitsch, and Stewart, Proc. Phys. Soc. (London) **70**, 110 (1957).
Br 30 H. C. Brinkman and H. A. Kramers, Proc. Acad. Sci. Amsterdam **33**, 973 (1930).
Br 51 Brunings, Knipp, and Teller, Phys. Rev. **60**, 657 (1951).
Br 54 Bransden, Delgarno, and King, Proc. Phys. Soc. (London) **67**, 663 (1954).
De 54 A. Delgarno, Proc. Phys. Soc. (London) **67**, 1010 (1954).
Dm 57 I. S. Dmitriev, J. Exptl. Theort. Phys. (U.S.S.R) **5**, 473 (1957); Zhur. Eksptl. i Teort. Fiz. **32**, 570 (1957).
Fi 51 O. B. Firsov, J. Exptl. Theort. Phys. **21**, 1001 (1924).
Fo 24 R. H. Fowler, Phil. Mag. **47**, 416 (1924).
Ge 56 V. I. Gerasimenko and L. N. Rosentsveig, Zhur. Eksptl. i Teort. Fiz. **31**, 684 (1956); English transl. Soviet Phys. JETP **4**, 509 (1957).
Ja 53 J. D. Jackson and H. Schiff, Phys. Rev. **89**, 359 (1953).
Kn 41 J. Knipp and E. Teller, Phys. Rev. **59**, 659 (1941).
Mo 56 B. L. Moiseiwitsch, Proc. Phys. Soc. (London) **A69**, 653 (1956).
Ne 54 J. Neufeld, Phys. Rev. **96**, 1470 (1954).
Op 28 J. R. Oppenheimer, Phys. Rev. **31**, 349 (1928).
Pr 57 T. Pradhan, Phys. Rev. **105**, 1250 (1957).
Ta 55 K. Takayangi, Sci. Repts. Saitama Univ. **II**, 33 (1955).
Th 27 L. H. Thomas, Proc. Roy. Soc. (London) **114**, 561 (1927).